Control Engineering Practice 145 (2024) 105847

Contents lists available at ScienceDirect

Control Engineering Practice

journal homepage: www.elsevier.com/locate/conengprac

A systematic management and control methodology for high energy saving in applications equipped with hydraulic servo-axes

Paolo Righettini [a,*], Roberto Strada [a], Monica Tiboni [b], Filippo Cortinovis [a], Jasmine Santinelli [a]

[a] Department of Engineering and Applied Sciences, University of Bergamo, Viale Marconi, 5, 24044 Dalmine, Italy
[b] Department of Mechanical and Industrial Engineering, University of Brescia, via Branze, 38, 25123 Brescia, Italy

ARTICLE INFO

MSC:
00-01
99-00

Keywords:
Hydraulic servo-axis
Management and control of hydraulic actuator
Hydraulic dynamic modelling
Energy saving
Hydraulic energy optimizer
Controlled hydraulic power supply
Carbon foot-print

ABSTRACT

A systematic methodology for the real-time improvement of the overall efficiency of applications using hydraulic servo-axes is presented. The proposed methodology introduces three modules: a hydraulic actuator load estimator, a hydraulic energy optimizer and a controlled hydraulic power supply; these are discussed at the theoretical and application level. The proposed approach reduces the power losses across the main elements of the hydraulic circuit, leading to high energy savings and introducing a new guideline on managing and controlling the servo hydraulic actuator. The methodology is applicable to any application using hydraulic servo-axis systems, and therefore it is not tailored to a particular field. Its performances have been evaluated in different industrial case studies (a blanking press, a drawing press and a die-casting plant) through numerical simulations. Conspicuous energy savings, ranging between 59% and 88%, have been obtained in simulation, suggesting that a significant carbon footprint reduction for energy-intensive hydraulic machinery is achievable in a wide range of applications.

1. Introduction

The development of hydraulic systems has recently focused on efficiency improvement and energy saving, which are today important research topics (Duflou et al., 2012; Mahato & Ghoshal, 2020). In all fields involving high energy consumption, numerous studies have been made to reduce emissions and save energy, as a result of ever-increasing energy needs, industry's need to reduce CO_2 emissions, rising electrical energy costs, rigorous administrative restrictions (Koivumäki et al., 2019; Schmidt et al., 2015), and environmental concerns (Göttlicher & Pruschek, 1997; Xie & Li, 2021).

The energy consumption is a key determinant of the emission of polluting gases. Wackernagel and Rees (1998) of the University of British Columbia introduced for the first time the concept of an Ecological Footprint. Subsequently, the Carbon Footprint parameter, used to estimate greenhouse gas emissions, has been introduced. The Kyoto Protocol of 1997 established which greenhouse gases must be taken into account when calculating the Carbon Footprint. A technical standard was developed to evaluate the carbon footprint of a product or service: UNI CEN ISO/TS 14067:2014 "Greenhouse gases – Product carbon footprint – Requirements and guidelines for quantifying and communication", which came into force on September 11, 2014. The carbon footprint is the parameter that makes it possible to determine the impact of anthropic activities on climate change, better than any other. Indeed, the parameter makes it possible to estimate the greenhouse gas emissions into the atmosphere caused by a product, a service, an organization, an event or a person, generally expressed in tons of equivalent CO_2, calculated over the entire life cycle of the analysed system.

Applications in the fields of heavy manufacturing, transportation, building, agriculture, earth moving, and aerospace widely employ hydraulic fluid power systems, owing to their ability to apply high forces, to directly drive the load, and to their ruggedness and shock tolerance resulting from the absence of reduction gears. Further advantages of hydraulic systems are their high energy density and their ability to generate very high power, as noted in Dindorf and Wos (2020).

In 2012, Oak Ridge National Laboratory (ORNL) published a report on a study that aimed to provide a rough estimate of the U.S. consumption, emissions, and efficiency of fluid-powered systems. ORNL cooperated with the National Fluid Power Association (NFPA) and 31 industrial partners to collect data for this evaluation. The results of the study, summarized in Table 1, show that the energy efficiency of hydraulic fluid power systems is very poor, as demonstrated also by several authors like Wang and Wang (2014). Consequently, there are

* Corresponding author.
E-mail addresses: paolo.righettini@unibg.it (P. Righettini), roberto.strada@unibg.it (R. Strada), monica.tiboni@unibs.it (M. Tiboni), filippo.cortinovis@unibg.it (F. Cortinovis), jasmine.santinelli@unibg.it (J. Santinelli).

https://doi.org/10.1016/j.conengprac.2024.105847
Received 29 June 2023; Received in revised form 22 November 2023; Accepted 10 January 2024
Available online 13 January 2024

Table 1
Estimated impact (energy, emissions and economics) of the U.S. fluid power industry (Alles et al., 2012).

Sector	Energy consumption [10^{15} kJ/Year]	Emissions [10^{9} kg CO_2]	Average efficiency [%]
Agriculture and construction industries	0.36	26.32	21.1
Fluid powered off-road vehicles	1.26	91.73	21.1
Industrial Hydraulics	1.09	196.12	50
Aerospace Hydraulics	0.024	1.71	n.a.

wide margins for energy efficiency improvement and carbon footprint reduction in applications relying on hydraulic systems.

For many years, academics and businesses have been focusing on increasing the energy efficiency of hydraulic drives and systems, and this trend has accelerated in the last four to five years. In the context of energy depletion (Wang et al., 2022), low system efficiency is a critical issue that must not be ignored.

A review of the most important approaches to energy saving in hydraulic drive systems can be found in Mahato and Ghoshal (2020). They identified four main categories: hybridization, waste energy recovery, energy loss reduction, and control algorithms. Hydraulics consists of two main areas: mobile and stationary, depending on the intended use. The circuital architectures adopted for both areas usually differ significantly, therefore the proposed solutions for energy saving are also different. Given the variety and complexity of hydraulic systems, the approaches summarized by Mahato and Ghoshal (2020) are joined by a multitude of different solutions, characterized by particular plant architectures and specific control techniques and algorithms. Hybridization is used in mobile applications and involves the creation of systems in which different technologies are used simultaneously for the same movement, in parallel or series configuration, as well as the use of energy storage solutions for the best possible management of the system's energy needs. Another strategy for waste energy recovery in the mobile field is regenerative braking systems. For the reduction of energy losses of stationary hydraulic systems, studies focus more on throttling energy loss reduction than on mitigation of other energy losses, such as frictional and leakage losses, compressibility losses, and losses due to pressure drop in pipes and fittings (Mahato & Ghoshal, 2020). Some researchers propose innovative solutions for system architecture, some for control, and some for both.

Some interesting studies that present energy saving solutions for hydraulic systems are described below. Dindorf and Wos (2020) presented three novel energy-efficient power supply solutions for hydraulic forging machines: the first is based on multiplier pump system with a piston oil pump and two oil/water piston multipliers; the second solution is based on the series and in parallel connection of a set of pumps, and the third uses two parallel supply circuits. Furthermore, the authors investigated and implemented real-time model predictive control, based on multiple inputs multiple outputs and global predictive control, on an 80 MN industrial hydraulic press. In order to produce large steel forgings of good quality, the control parameters of the hydraulic press are selected based on predictions of the parameters of the hot open die forging process. This results in lower consumption of electricity, gas, and working fluid as well as lower noise emissions from pumping systems.

Koitto et al. (2018) studied the application of a Direct Driven Hydraulics (DDH) unit for an industrial high load lifting system. This is a method based on a pump-controlled closed system. This technology if often used for traction control of mobile machinery, whereas it is less common in stationary industrial applications, where the prime mover is almost always an electric motor, and valve-controlled open systems are usually favoured. This is because pump-controlled systems usually have only one actuator, but large open system centralized hydraulic installations for stationary applications typically have several actuators. However, purely pump-controlled systems have become increasingly popular also for stationary applications over the last 20 years. This trend is a result of the need for greater energy efficiency and the favourable technical and cost development of electric drives. Three different variants of DDH were considered: plain DDH, DDH with load compensation, and DDH with load compensation and vibration damping. In terms of energy consumption, each of these systems outperformed the simulated valve-controlled system, with energy savings varying between 53%–87%. However, the dynamics and stability of the system are not satisfactory, as vibrations are generated both during movement and when reaching the target position.

Designing optimal control algorithms to minimize energy consumption is one of the greatest challenges in modern control theory, and this also applies to Hydraulic Servo Actuator (HSA) control. With this aim, Djordjevic et al. (2023) developed an event-triggered data-driven optimal controller for HSAs with completely unknown dynamics, based on an adaptive dynamic programming framework, and operating via output feedback. The proposed approach does not require modelling the entire system dynamics. Under real conditions, an accurate determination of the parameters is impossible due to nonlinear sources present in HSAs. A linear discrete model of HSAs is considered, and an online learning data-driven controller is used, which is based on measured input and output data instead of non-measurable states and unknown system parameters. Further approaches to define optimized control algorithms to minimize energy or manage unknown system parameters can be found in Song et al. (2023) and Zhou et al. (2022).

One control technique for an asymmetric cylinder that has shown a significant improvement in energy efficiency without compromising dynamic performance is the separate meter-in separate meter-out (SMISMO) control set-up. Koivumäki et al. (2019) adopted this approach for a hydraulic robotic manipulator. A modular Virtual Decomposition Control (VDC) is combined with the SMISMO controller. By virtually decomposing the original system into modular subsystems (objects and open chains) in VDC, the control design and stability analysis can be performed at the subsystem level without the need for further approximations. The energy saving achieved for a redundant manipulator, with three-DOF, a maximum reach of 4.2 m, and a payload of 475 kg, is 45% compared with a conventional servovalve control.

In a hydraulic lifting system, the introduction of a bypass valve that can only open during the downward stroke leads to an improvement in energy efficiency, as demonstrated by Rana et al. (2022). According to the study, energy efficiency is higher at lower operating pressures and decreases steadily with increasing working pressure. With higher loads, the energy efficiency is inversely related to the operating pressure. Electro-Hydraulic Actuators (EHAs) are normally developed with a closed circuit. Ho and Le (2021) proposed an EHA solution based on an open circuit, in which the outlet port of the cylinder and suction port of the pump are directly connected to the tank. The results of simulations and experiments show that the system can reduce energy consumption by about 20% when compared to a conventional valve-controlled hydraulic system without energy recovery EHA.

A hybrid architecture, an electro-hydraulic servo system with an EHA and a valve-controlled hydraulic system is presented by Niu et al. (2021). This solution consists of a fixed displacement pump driven by a servo motor and by a multi-functional valve control system with two proportional directional control valves and four switching valves. By using supply pressure controllers based on disturbance observers and flow controllers based on grey predictors, the authors achieved significant energy savings (flow loss was reduced by more than half) under complex load conditions.

A similar approach is presented in Lyu et al. (2019), with a configuration that combines independent meter-in and meter-out valves control approach and direct pump control, by taking advantage of their respective strengths, to simultaneously achieve high energy efficiency and excellent motion performance. The reference trajectory velocity feed-forward approach is used to control the pump, which supplies the bulk of the flow rate driving the cylinder. To ensure the required tracking performance, closed-loop controlled independent metering valves are used to precisely control the remainder amount of the flow rate. Since only a tiny portion of the flow rate is throttled, throttling losses are expected to be significantly lower than in other systems proposed in the literature. In addition, the pump's feed-forward controller is quite simple and the efficiency of the tracking is guaranteed.

A hybrid solution has been proposed by others, such as in Helian et al. (2021). When a hydraulic actuator operates under negative loads and if the return side of the actuator does not have enough meter-out damping, it cannot accurately follow the intended trajectory. While this is happening, the pressure in the pump-connected chamber might drop dramatically and reach a very low level, which can lead to nonlinear phenomena such as cavitation and actuator vibration. This could make the motion control of the actuator unstable. In addition, the hydraulic components can be damaged by cavitation in the cylinder chamber. In conventional EHAs, an accumulator is used to prevent cavitation and suction under negative loads. This accumulator maintains the pressure and compensates for the fluid loss. As a result of the lack of meter-out damping, this design requires additional hardware auxiliaries and also makes the equipment more susceptible to load fluctuations. Helian et al. (2021) proposed a solution to the problem with an actuator driven by a servomotor pump and a proportional valve to control the meter-out pressure.

Special solutions have been proposed for hydraulic presses, which are characterized by very low energy efficiencies. As estimated by Zhao et al. (2015), about only 10% of the power fed into the system is useful for the forming process. For presses with multiple motor-pumps, Huang et al. (2019) focus on the problem of high energy consumption caused by the pump unloading. They propose an energy-saving design method for the drive system based on minimizing an idling index. The results show that the installed power has decreased by 41.72%, and the energy consumption of the drive system during a working cycle has been reduced by 26.97%.

Li et al. (2017) presented an energy-saving solution for a multi-press system based on the combination of multiple presses, that share the drive system and thus the motor pumps. The combination of presses makes it possible to use the excess energy of one press as input energy for the other during some operations, improving the energy efficiency of the drive system and utilizing potential energy directly. The technology was applied to two hydraulic presses in a tandem line, and the results show that a single press can save 36% of electrical energy in the forming processes studied.

Therefore, the state-of-the-art of research concerning the efficiency improvement of hydraulically powered systems regards mainly the optimization of a particular application case, where the optimization process involves some of the components of the hydraulic circuit. In some cases, the authors propose the introduction of a dedicated power supply to follow the non-constant power required by the load, in other cases an optimization of the circuit or the introduction of waste energy recovery to increase the overall efficiency. Other authors propose an optimized control approach using a conventional hydraulic scheme. The state-of-the-art in this field does not offer a general approach to increasing the efficiency of a system driven by a hydraulic actuator.

The literature also shows a comprehensive scientific production discussing approaches for managing and controlling complex systems, mainly having electric actuators, whose application field differs from the one discussed in this paper. As an example, these recent works concerning actuators employed in different fields (Meng, Yu, Zhang & Yang, 2023; Su & Xiao, 2021), robotic applications (Al-Shuka & Mikolajczyk, 2023; Guo et al., 2023; Tran et al., 2023) and complex systems (Ahmadi et al., 2023; Meng, Yu, & Zhang, 2023; Zare et al., 2023) address control of actuators, the related uncertainties, disturbances and faults estimation and management. The scientific investigation in these fields may represent a scientific knowledge base for the development of a methodology for management and control applications equipped with hydraulic servo-axes.

This paper proposes a new systematic methodology for real-time efficiency improvement of a system driven by a hydraulic actuator with the aim of reducing losses in the circuit. The proposed approach is introduced considering an actuator for motion control commonly used in industrial applications, but the concept is more general and may be applied in other configurations. The methodology also introduces a new control scheme for motion control with a hydraulic actuator, based on the regulation of both the hydraulic power supply and the proportional valve of the actuator.

The article is structured as follows: the discussion of the theory underlying the proposed methodology is detailed in paragraph 2; paragraph 3 is dedicated to the presentation of the system considered in the simulations and the report on the computational results; paragraph 4 discusses the simulation results and compares the energy consumption obtained with different variations of the methodology. Finally, the conclusions are reported: the impact of the proposed method on the reduction of absorbed energy and CO_2 emissions is highlighted, and possible further developments of the work are explained.

2. Methodology

The main components of a hydraulic system are a pump driven by a prime mover (electric motor in industrial hydraulics and internal combustion engine in mobile hydraulics and aerospace), control valves, hydraulic lines, and actuators. These elements are a source of power losses and inefficiencies whose contribution also depends on the architecture of the system. Hoses, pipelines, and control valves deliver the pressurized fluid to the actuators. They exhibit inefficiencies due to internal leakage (tare flow) and pressure drops depending on the flow rate, the load condition, and supply pressure of the valve.

This work proposes a methodology for real time efficiency improvement of a system driven by a hydraulic actuator. This target is reached through the management of the hydraulic circuit components responsible for the control of the hydraulic actuator: the Hydraulic Power Supply (HPS) and the Actuator Proportional Valve (APV) regulating the fluid flow into the actuator. The methodology increases the overall efficiency reducing the power losses on the principal hydraulic circuit elements.

The methodology's presentation considers a motion control application whose actuator is linear (Fig. 1), representing a typical configuration of an industrial application requiring high forces for the execution of the working action. In these applications, the bandwidth required for the motion control system is often high. Therefore, the proposed real-time methodology developed to increase the system efficiency requires a suitable system model. Fig. 1 shows the relevant elements of a controlled hydraulic linear actuator.

The block HPS generates the supply pressure P_S; the Motion Profile Generator (MPG) generates the motion position profile and its relevant time derivatives as a function of time; the APV regulates the flow into the actuator and the Hydraulic Actuator Regulator (HAR) is the motion controller.

The dynamic model of the system shown in Fig. 2 is represented by the system of equations (1); it includes the mechanical dynamic equilibrium at the actuator, the continuity equations of the flow entering and leaving the cylinder chambers, and the characteristic equations of

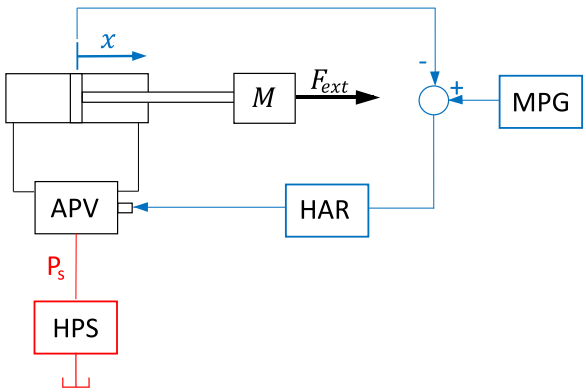

Fig. 1. Motion controller scheme for a linear hydraulic actuator: Motion Profile Generator (MPG), Hydraulic Actuator Regulator (HAR), Actuator Proportional Valve (APV), Hydraulic Power Supply (HPS).

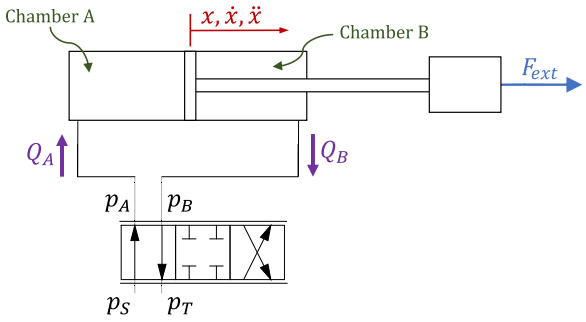

Fig. 2. Diagram of the cylinder-valve system with indication of the main variables.

the flow paths of APV (Aboelela et al., 2018; Akers et al., 2006; Jelali & Kroll, 2002; Righettini et al., 2018).

$$\begin{cases} m\ddot{x} + c\dot{x} = P_A A_A - P_B A_B + F_{ext} \\ Q_A = C_i\left(P_A - P_B\right) + C_e P_A + A_A\dot{x} + \dfrac{\dot{P}_A}{\beta} V_A(x) \\ Q_B = -C_i\left(P_A - P_B\right) + C_e P_B - A_B\dot{x} + \dfrac{\dot{P}_B}{\beta} V_B(x) \\ Q_A = \text{sign}\left(\Delta P_{CA}\right) K_A H \sqrt{\left|\Delta P_{CA}\right|} \\ Q_B = -\text{sign}\left(\Delta P_{CB}\right) K_B H \sqrt{\left|\Delta P_{CB}\right|} \end{cases} \tag{1}$$

In the system of equations (1), m and c are the mass and damping coefficient of the cylinder, while A_A and A_B are the piston's cross-section areas corresponding respectively to chamber A and chamber B. P_A and P_B are the pressures acting in cylinder's chamber A and B respectively; likewise, Q_A and Q_B are the inlet flow rates in the chambers A and B. $V_A(x)$ and $V_B(x)$ are the volumes of chamber A and B respectively; their dependence on x is $V_A(x) = V_{0A} + A_A x$ and $V_B(x) = V_{0B} - A_B x$, where V_{0A} and V_{0B} are the volumes of the two chambers when $x = 0$. C_i and C_e are respectively the internal and external leakage coefficients of the cylinder; β is the fluid's bulk modulus. H is a non-dimensional parameter included in the interval $[-1, 1]$ representing the spool position regulation, while K_A and K_B are coefficients whose value varies with the valve type and size and can be derived from the characteristic curves specified by the manufacturer ΔP_{CA}, ΔP_{CB} are the pressure drops across the valve's ways; they depend on H, P_S, P_A, P_B: $\Delta P_{CA} = \Delta P_{CA}\left(H, P_S, P_A\right)$, $\Delta P_{CB} = \Delta P_{CB}\left(H, P_S, P_B\right)$.

The system of equations (1) may also expressed in more compact form:

$$\dot{\bar{\mathbf{x}}} = \mathbf{A}\left(\bar{\mathbf{x}}\right)\bar{\mathbf{x}} + \mathbf{B}\left(\bar{\mathbf{x}}, \bar{\mathbf{u}}\right) \quad , \quad \bar{\mathbf{x}} = \begin{bmatrix} x & \dot{x} & P_A & P_B \end{bmatrix}^T \tag{2}$$

where

$$\mathbf{A}\left(\bar{\mathbf{x}}\right) = \begin{bmatrix} 0 & 1 & 0 & 0 \\ 0 & -\dfrac{c}{m} & \dfrac{A_A}{m} & \dfrac{A_B}{m} \\ 0 & -\dfrac{A_A\beta}{V_A(x)} & -\dfrac{\left(C_i + C_e\right)\beta}{V_A(x)} & \dfrac{C_i\beta}{V_A(x)} \\ 0 & \dfrac{A_B\beta}{V_B(x)} & \dfrac{C_i\beta}{V_B(x)} & -\dfrac{\left(C_i + C_e\right)\beta}{V_B(x)} \end{bmatrix} \tag{3}$$

$$\mathbf{B}\left(\bar{\mathbf{x}}, \bar{\mathbf{u}}\right) = \begin{bmatrix} 0 & \dfrac{F_{ext}}{m} & \dfrac{Q_A\beta}{V_A(x)} & \dfrac{Q_B\beta}{V_B(x)} \end{bmatrix}^T \tag{4}$$

$$\bar{\mathbf{u}} = \begin{bmatrix} H & P_S \end{bmatrix}^T \tag{5}$$

The choice of the input vector, which is composed of the valve command input H, the only one commonly used in hydraulic servo-axes, and the pressure supply P_S, outlines that the behaviour of the dynamic system can be controlled by acting on both the proportional valve opening and the pressure supply.

Without loss of generality, for the discussion of the methodology, a system is considered in which the chambers of the cylinder are symmetrical, i.e. $A_A = A_B = A$, and an origin of the position coordinate x such that $V_{0A} = V_{0B} = V_0$. With these assumptions, introducing the control flow Q_L, i.e. the flow provided by the APV through the load evaluated as $\left(Q_A - Q_B\right)/2$, and the pressure drop across the chambers of the cylinder $P_L = P_A - P_B$ (Akers et al., 2006; Righettini et al., 2016, 2017), the system of equations (2) can be written in the form:

$$\dot{\tilde{\mathbf{z}}} = \tilde{\mathbf{A}}\bar{\mathbf{z}} + \tilde{\mathbf{B}}\left(\bar{\mathbf{z}}, \bar{\mathbf{u}}\right) \quad , \quad \bar{\mathbf{z}} = \begin{bmatrix} x & \dot{x} & P_L \end{bmatrix}^T \tag{6}$$

where

$$\tilde{\mathbf{A}} = \begin{bmatrix} 0 & 1 & 0 \\ 0 & -\dfrac{c}{m} & \dfrac{A}{m} \\ 0 & -\dfrac{2A\beta}{V_0} & -\dfrac{2C_i\beta}{V_0} \end{bmatrix} \tag{7}$$

$$\tilde{\mathbf{B}}\left(\bar{\mathbf{z}}, \bar{\mathbf{u}}\right) = \begin{bmatrix} 0 & \dfrac{F_{ext}}{m} & \dfrac{2Q_L\beta}{V_0} \end{bmatrix}^T \tag{8}$$

$$\bar{\mathbf{u}} = \begin{bmatrix} H & P_S \end{bmatrix}^T ; \tag{9}$$

As shown by Rydberg (2016), the instantaneous value of the flow Q_L can be modelled, for a critical centre spool valve, as $Q_L = KH\sqrt{P_S - \text{sign}(H)P_L}$.

Under the further assumption that the fluid is incompressible ($\beta \to \infty$), the system of equations (6) results:

$$\begin{cases} P_L = \dfrac{m\ddot{x} + c\dot{x} - F_{ext}}{A} \\ Q_L = C_t P_L + A\dot{x} \\ Q_L = KH\sqrt{P_S - \text{sign}(H)P_L} \end{cases} \tag{10}$$

The system of equations (10) shows that: first, the evaluation of the load pressure P_L depends on the knowledge of the mechanical load of the actuator; second, the evaluation of the flow rate Q_L depends on the knowledge of the kinematic state of the actuator; and third, the flow rate Q_L required to fulfil the current movement of the actuator and actuator's mechanical load state depends on both the valve opening H and the supply pressure P_S.

The last consideration outlines that there are ∞^1 solutions for the pair of valve opening H and supply pressure P_S that fulfil the application requirements regarding motion $\dot{x}$, $\ddot{x}$ and mechanical load.

As is known, in hydraulic servo-axis applications, the energy dissipation caused by the proportional valve depends on its pressure drop $P_V = P_S - \text{sign}(H)P_L$, and on the flow rate Q_L.

In most hydraulic applications, the supply pressure P_S is constant. In contrast, the line pressure P_L depends on the load condition of the actuator; therefore, the pressure drop P_V is a function of the load condition. The power loss is caused by the servo valve changes over

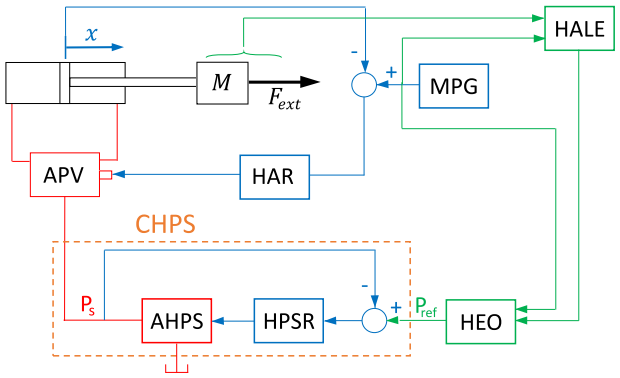

Fig. 3. Management and control methodology's functional blocks. Meaning of the colour based code: Red — hydraulic elements; Blue — control elements; Green: algorithmic elements. (For interpretation of the references to colour in this figure legend, the reader is referred to the web version of this article.)

time, and it increases as the supply pressure increases in relation to P_L.

This paper proposes a real-time methodology to reduce the power loss in the elements of the hydraulic circuit by acting on the valve opening H and pressure supply P_S. The choice of values for H and P_S, as presented in the discussion for the system of equations (10), is a trade-off between the power dissipation on the valve, the behaviour of the control valve, and the dynamic performances of the axis.

The proposed methodology requires the insertion of the Controlled Hydraulic Power Supply (CHPS) in the scheme shown in Fig. 1, which introduces a further variable for controlling the system, the supply pressure P_S, in addition to the commonly used valve command. In this scenario, the motion controller HAR defines the valve command as a function of the required motion profile MPG and the actual actuator motion. At the same time, the best possible energy saving depends on the selection of the setpoint for the pressure supply.

Three modules compose the proposed methodology, as shown in Fig. 3:

- Hydraulic Actuator Load Estimator (HALE): it is an algorithm that evaluates the load condition of the actuator;
- Hydraulic Efficiency Optimizer (HEO): it is an algorithm that determines the more suitable solution in P_S of the system of equations Eq. (2) or Eq. (6) as a function of the load and the kinematic state of the actuator, whose target is to minimize the power dissipation of the control valve while safeguarding the dynamic behaviour of the hydraulic actuator;
- CHPS: it is a controlled hydraulic power supply capable of generating the required supply pressures P_S. It consists of:
  - AHPS: it is a hydraulic power supply able to adjust the generated supply pressure by means of an appropriate command;
  - Hydraulic Power Supply Regulator (HPSR): it is the controller of the AHPS for obtaining the required supply pressure P_S.

The online determination of setpoint for the pressure supply to minimize power losses requires the two modules HALE and HEO, as their relationship represented in Fig. 3 shows.

The effectiveness of these modules in reducing power losses increases with increasing variability in the actuator's speed and force required for the application.

2.1. Hydraulic actuator load estimator

The HALE module determines the mechanical load F_{ml} of the hydraulic actuator for the desired movement and application. The first equation of the systems of equations (1) gives

$$P_A A_A - P_B A_B = -F_{ml} = m\ddot{x} + c\dot{x} - F_{ext} \tag{11}$$

For the simpler case described by the system of equations (10), the line pressure P_L directly depends on the actuator's mechanical load F_{ml}

$$P_L A = -F_{ml} = m\ddot{x} + c\dot{x} - F_{ext} \tag{12}$$

As shown in Fig. 3, the inputs of the HALE module are external forces, and the movement data of the load (speed and acceleration), while the output is the mechanical load of the actuator F_{ml}.

The algorithm for evaluating the mechanical load on the actuator F_{ml} can be based on different approaches depending on the type of load, the application, or the complexity of the estimation system used. Some of them may be:

1. an open-loop model which, as expressed by the first equation of the system (1), requires knowledge of all system parameters and external load, and which can be used, for example, in applications with periodic duty-cycles;
2. a real-time algorithm for the identification of F_{ml} based on the measure of the kinematic state of the actuator motion;
3. a real-time algorithm based on the force measure, the measure of the kinematic state of the actuator movement and system parameters;
4. other algorithm based on the measure of the pressure state of the two chambers of the cylinder;
5. or any other load estimator technique (e.g. based on parametric models as in Tutsoy et al., 2020).

Without loss of generality, this paper considers an open loop model of the load to determine F_{ml}.

2.2. Hydraulic efficiency optimizer

The HEO module determines the pressure supply that reduces the power losses across the servo valve. This pressure is the setpoint used by CHPS to supply the servo-axis.

The module is an algorithm that, knowing the mechanical load of the actuator F_{ml}, the actuator's kinematic state and using the system of equations (2) or (6), determines the optimal solution for minimizing the power losses.

Considering the simpler case described by the system of equations (10), the knowledge of the mechanical load of the actuator enables, with the help of Eq. (12), the direct evaluation of

$$P_L = \frac{-F_{ml}}{A}\,. \tag{13}$$

From the discussion of the system presented above (10) it is clear that its third equation allows the evaluation of the optimal supply pressure among the infinite number of possible ones.

In this paper, neither the type of optimization nor the best optimization criteria are examined or discussed. Instead, a direct, simple algorithm is proposed to determine the pressure setpoint for the CHPS based on characteristic equations of the servo valve as expressed by the third equation of the system of equations (10); solving it with respect to supply pressure P_S yields

$$P_S = \left(\frac{Q_L}{K\,H}\right)^2 + \mathrm{sign}(H)P_L \tag{14}$$

where the term

$$\left(\frac{Q_L}{K\,H}\right)^2 = P_V \tag{15}$$

represents the valve pressure drop. The power losses due to the servo valve are determined according to Eq. (16):

$$W_{loss} = P_V Q_L\,. \tag{16}$$

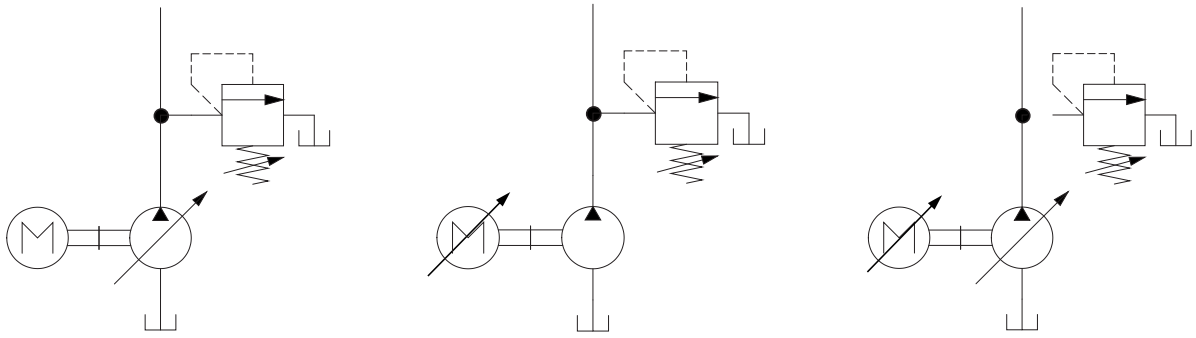

(a) Variable Displacement Fixed Speed (VDFS) (b) Servo-Pump Pressure Regulation (SPPR) (c) Variable Displacement Servo-Pump (VDSP)

Fig. 4. Adjustable Hydraulic Power Supply architectures.

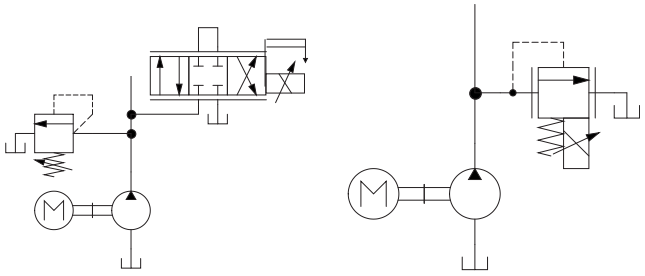

(a) Servo-relief Valve Pressure Regulation (SVPR) (b) Proportional Relief Valve (PRV)

Fig. 5. Adjustable Hydraulic Power Supply architectures.

Under the given hypotheses, the flow rate Q_L is proportional to the speed of the actuator $\dot{x}$ while P_V depends on the non-dimensional valve opening H.

According to Eq. (15) the pressure drop P_V decreases with increasing valve opening and, in the same way, Eq. (14) gives the minimum supply pressure that fulfils the kinematic and force requirement for the actuator, respectively represented by flow line Q_L and pressure line P_L.

The determination of the supply pressure P_s using Eq. (14) requires knowledge of both H and P_L. The line pressure P_L depends on the mechanical load of the actuator F_{ml}, which is evaluated by the HALE module. This calculation may be subject to uncertainties due to the model or methodology used. The term $\text{sign}(H)$ defines the position of the valve spool, positive when the valve connects the pressure supply to chamber A, and negative when the valve connects the pressure supply to chamber B. The position of the valve spool (the sign of H) depends on the motion requirements, being generally determined by the power flow across the actuator, given by

$$W_L = -F_{ml}\dot{x} \ . \tag{17}$$

This paper assumes that the valve feeds chamber A when the power flow is positive and chamber B when the power flow is negative. Under this assumption, Eq. (14) can be rewritten using Eq. (17) in the following form

$$P_S = \left(\frac{Q_L}{K\,H}\right)^2 + \text{sign}(W_L)P_L \tag{18}$$

The evaluation of the supply pressure P_S using Eq. (18) requires the definition of the value of H through an optimization method. This paper does not propose a specific energy waste minimization algorithm. Instead, for the presentation of the methodology, it introduces a suitable constant value H^* based on the analysis of Eq. (15). This shows that the power losses at the servo valve can be reduced with high values of H, suggesting the use of the servo valve spool in a high opening position.

Table 2
Qualitative comparison of the considered architectures for the fluid power generation system. Electric Drive Cost (EDC); Pump Control Dynamics (PCD); System Control Dynamics (SCD).

Arch.		Pump cost	EDC	PCD	SCD	Overall cost
VDFS	FS – VD	High	Low	Slow	Slow	Medium
SPPR	VS – FD	Low	High	–	Slow/Medium	Medium/High
VDSP	VS – VD	High	High	Slow	Medium	Very High
SVPR	FS – FD + SRV	Low	Low	–	Fast	Low
PRV	FS – FD + PPRV	Low	Low	–	Slow	Low

The value of H^* must be high enough to achieve an appropriate energy saving, and low enough to ensure the regulation capability of the motion controller HAR. Once a suitable value for H^* has been determined, Eq. (19) calculates the reference supply pressure required by the system to fulfil the motion and load requirements

$$P_{S_{ref}} = \left(\frac{Q_L}{K\,H^*}\right)^2 + \text{sign}(P_L\dot{x})P_L \ . \tag{19}$$

2.3. Controlled hydraulic power supply

The proposed methodology introduces the concept of a controlled power supply, i.e. a hydraulic flow generator that can generate flow at a given pressure. The methodology requires a response time of the controlled supply pressure that is less than the variation time of the line pressure P_L and the speed required for the application. Therefore, the choice of the controlled power supply depends on the force and speed time profile of the actuator required by the specific application. For instance, the Ideal Pressure Source (IPS) is a device with infinite bandwidth and unitary efficiency, and is therefore able to guarantee the desired time profile of the supply pressure without wasting energy.

In the following, the paragraph presents some AHPS architectures that can be used for building the Controlled Hydraulic Power Supply.

Several well-known power supply architectures allow adjusting the supply pressure using open or closed loop configuration. Two of these are Variable Displacement Fixed Speed (VDFS) shown in Fig. 4(a) and Proportional Relief Valve (PRV) shown in Fig. 5(b).

The VDFS architecture has a Variable Displacement (VD) pump and an electric drive Fixed Speed (FS) (asynchronous motor connected directly to the power supply). The swivel angle of the pump regulates the pressure level via an internal or external control loop based on a pressure sensor. Due to the mechanical pump's configuration, the bandwidth of the pressure level is between 1 and 3 Hz for commercially available devices. In addition, the cost of the VD pump is higher than that of the fixed displacement pump.

The PRV architecture has a fixed displacement pump, a fixed speed electric drive and Proportional Relief Valve to control the supply pressure. The bandwidth of this controlled power supply is higher than the previous one, and is between 3 to 6 Hz for commercial devices.

The SPPR architecture shown in Fig. 4(b) consists of a fixed displacement pump driven by a servo-motor (asynchronous motor powered by an inverter with flux vector control or a brushless servo-motor). It controls the supply pressure by adjusting the torque exerted by the electric drive. The Variable Displacement Servo-Pump (VDSP) architecture shown in Fig. 4(c) has a VD pump driven by a servo-motor. It controls the pressure supply by adjusting the torque exerted by the electric drive and the displacement of the pump. However, the cost of these solutions is high, especially for powers of several tens of kW. The bandwidth of the pressure level of these solutions is relatively low for commercial devices and is in the order of a few Hertz. On the other hand, the bandwidth of the architecture SPPR can be increased with a brushless servo motor as an electric drive that guarantees the required speed and torque profiles. The appropriate servo-motor and drive can be designed according to the methodology described in Righettini et al. (2022).

The SVPR architecture shown in Fig. 5(a) has a fixed displacement pump and a fixed speed electric drive (asynchronous motor connected directly to the power supply), as well as a servo-valve to control the power supply pressure. This architecture extends the dynamic performance of the PRV one, using a suitable servo-valve to discharge the flow, and regulating it using a control loop on the supply pressure. The bandwidth of this architecture is the highest of the pressure supplies presented here, thanks to the introduction of the high dynamic servovalve like those used to control the actuator's motion. This architecture does not alter the configuration of a hydraulic power supply with a Fixed Displacement (FD) pump. It only introduces a new high dynamic discharging valve into the hydraulic circuit, so that the proposed solution can be installed in both new and existing plants. Table 2 summarizes a qualitative comparison among the previously discussed solutions for the fluid power generation system, taking into account efficiency, costs and dynamic performance.

Among the power generation architectures presented, the SPPR and SVPR solutions enable higher dynamic performances without significant additional costs. Therefore, they may be particularly suitable and economically favourable in hydraulic applications with dynamic loads that change rapidly over time, which is a typical situation of many industrial applications. In addition, SVPR architecture has a lower impact on the cost and complexity of the system compared to SPPR, as it only requires the introduction of a servo-relief proportional valve in a conventional system.

3. Simulations and results

This section describes the simulations in which the methodology presented in Section 2 was applied to three industrial cases, with the intention of highlighting the achievable energy savings. The case studies involve machinery widely used in the industrial field: a blanking press, a die-casting machine, and a drawing press. The actuator's motion and working force–time profiles used in the simulations have been defined by the information collected from the literature and from companies operating in the industrial hydraulic field (Adamane et al., 2015; Dalquist & Gutowski, 2004; Li et al., 2017; Xu et al., 2020). In addition, only the cycle phases relating to the actuator were considered for the three processes, and phases such as work-piece loading or unloading, which are necessary for the cycle but do not involve the actuator, were neglected. Although these phases affect the overall cycle time, they do not affect the potential efficiency and energy savings that can be achieved with the proposed techniques.

As discussed in the previous section, the main innovations of the proposed methodology are based on three components: the CHPS, the HALE, and the HEO.

The HALE module used in the simulations to estimate the mechanical load F_{ml} is an algorithm consisting of a parametric model of the system expressed in Eq. (12), based on the evaluation of the viscous, inertial forces and the knowledge of the external force. The knowledge

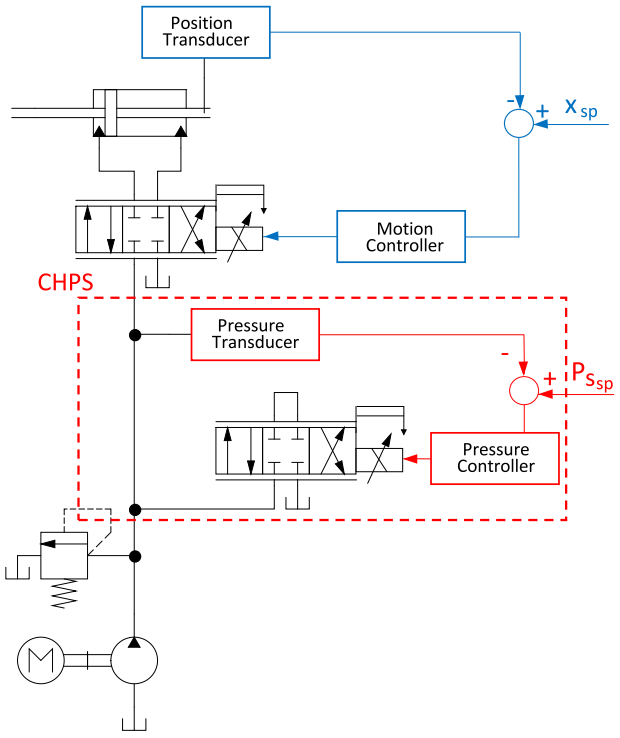

Fig. 6. Control scheme with CHPS based on Servo-relief Valve Pressure Regulation.

of the external force derives from the measurable and cyclic nature of the application. It can be known as a function of the time or the actuator's displacement.

The HEO module implemented in simulations is not based on a specific cost function or optimization procedure; instead, a constant value $H^* = 0.75$ in Eq. (15) was chosen to achieve a balance between energy saving and dynamic performance of the position controller. Given F_{ml} and H^*, it is possible to evaluate P_S according to Eq. (19). This value of H^* is not optimal, but this simple choice makes it possible to implement the proposed method and achieve high energy savings.

Finally, for each case study different hydraulic pressure supplies were adopted. Considering the highly dynamic requirements of the applications, the presented simulations mainly concern the SPPR and the SVPR, for which the following quantities are reported:

- input and output quantities for the HALE and HEO modules;
- set-point and actual supply pressure;
- set-point and actual piston position and speed;
- nominal and actual flow rate towards the actuator;
- actuator's servo-valve percentage opening;
- opening of servo-valve for pressure control (only for SVPR);
- discharged flow-rate (only for SVPR);
- input and wasted energy.

Figs. 6 and 7 present the general scheme of the investigated cases, where the resulting CHPS and the controlled linear actuator are shown for the two hydraulic power supply architectures considered in the simulations. The system therefore has two independent control loops, one for controlling the actuator motion and one for controlling the power supply.

The following sections provide a detailed analysis of each case study, accompanied by graphical representations and commentary on the simulation results. All simulated cases consist of the same hydraulic components, among which the double rod cylinder, actuator servo-valve, and fixed displacement internal gear pump are the most

Table 3
Technical data and parameters of the main elements of the hydraulic circuit considered in simulation model.

Circuit element	Parameter	Value
Pump	Code	Bosch-Rexroth PGH4-3X/020
	Type	Fixed Displacement Internal Gear Pump
	Displacement	20.1 [cm^3/rev]
	Nominal Flow rate	28.9 [l/min] (at 1450 RPM, 10 bar)
	Speed Range	200–3000 [RPM]
	Nominal Continuous Pressure	315 [bar]
Servo-Valve	Code	Bosch-Rexroth 4WS2EM6-2X/20B11ET315K17EV
	Type	Pilot operated Proportional 4/3 open centre
	Nominal flow rate	20 [l/min] (Δp = 70 bar)
	Maximum flow rate	40 [l/min] (Δp = 300 bar)
Cylinder	Code	Bosch-Rexroth CGH2MT4/50/36/480A30/H11CFUT
	Type	Double Acting, through rod cylinder
	Cylinder bore	50 [mm]
	Rod diameter	36 [mm]
	Stroke	480 [mm]

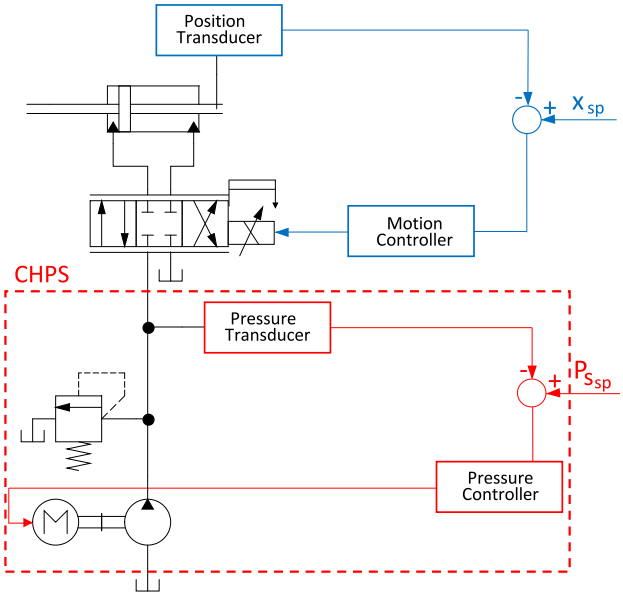

Fig. 7. Control scheme with CHPS based on Servo-Pump Pressure Regulation.

relevant. Table 3 summarizes the most important technical data of these components of the hydraulic circuit.

The tool used for developing the numerical simulations is MathWorks Simscape. As an example, Figs. 8(a) and 8(b) represent the sub-models of the actuator and of the SVPR power supply architecture.

3.1. Blanking press case study

The complexity of workpiece structures and the difficulties of stamping have increased in recent years, so that fine blanking presses with hydraulic power transmission are attracting more and more attention. According to reports, more than 300 car parts have been produced using fine blanking technology.

As described by Xu et al. (2020), a typical blanking process comprises five main phases:

- **fast approaching**: phase of rapid approach to the workpiece in which the rod performs part of the downward stroke and encounters no resistance during translation;
- **deceleration and blanking**: when the rod tooling comes into contact with the workpiece, there is a sudden deceleration that brings the translation speed to a value close to zero in a very short time; the pressure of the fluid increases until it overcomes the yield strength of the material of the workpiece and the blanking phase begins. A simplified and precautionary model of the process is considered: it is assumed that after the rapid descent phase, blanking begins at a constant speed, while the external load is assumed to be constant;
- **ejection**: once the blanking is finished, the downward stroke continues promoting the ejection phase of the semi-finished product. The resistance that occurs during this process is very low, and can be neglected. The piston moves in the same way as during rapid descent. As this is a short phase, a speed equal to that of the blanking phase is considered;
- **fast returning**: fast return to the bottom dead centre.

Fig. 9 shows the quantities that characterize the inputs and outputs of the HALE and HEO modules. Fig. 9(a) shows the inputs of the HALE module; in the proposed implementation, the required elements are: the external forces, which are assumed to be known due to the cyclic and measurable nature of the application; the velocity setpoint multiplied by a coefficient c, which provides an estimate of the viscous friction forces that will occur during the motion; and the acceleration setpoint multiplied by a mass coefficient m, which is an estimate of the inertial forces that will occur during the blanking cycle. The mass and friction coefficients derive from a suitably developed lumped-parameter model of the actuator. The output of the HALE module, represented in Fig. 9(b), consists of an estimate of the mechanical load F_{ml}. This estimate is required by the HEO module, whose additional inputs, represented in Fig. 9(c), are estimates of the line volumetric flow Q_L and the power W_L as required in Eq. (18). In the presented implementation, the flow rate estimate is obtained from the piston velocity setpoint multiplied by the piston area, whereas W_L is approximated by the product of $F_{ml,estimate}$ and $-\dot{x}_{sp}$. The output of the HEO module, shown in Fig. 9(d) is the supply pressure setpoint $P_{S,sp}$. Given this description, it can be remarked that, all in all, the HALE and HEO modules developed here only require reference quantities, a parametric model of the actuator, and an estimate of the external forces. Their operation is therefore not influenced by the technical solution chosen for the implementation of the CHPS.

Concerning the relationship between the inputs and outputs of the HALE module, it can be seen that the external load in the initial and final phases of the cycle is gravitational and comparable in magnitude to the inertial and viscous loads. On the contrary, the blanking force is clearly dominant in the middle phase. As regards the HEO module inputs, it can be seen in Fig. 9(c) that the power W_L is negative in the initial phase; this is because the external gravitational action aids the downward movement of the piston. The sign of W_L becomes positive during the blanking operation, then negative during the ejection of the blank, and finally positive during the return phase, in which gravity counteracts the movement. Fig. 9(d) shows the generated supply pressure setpoint; it can be seen that the maximum value is clearly

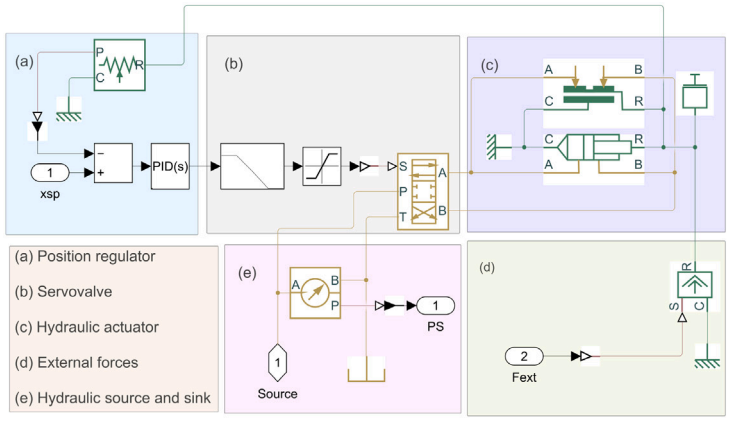

(a) Simscape scheme of the servo-valve/actuator system.

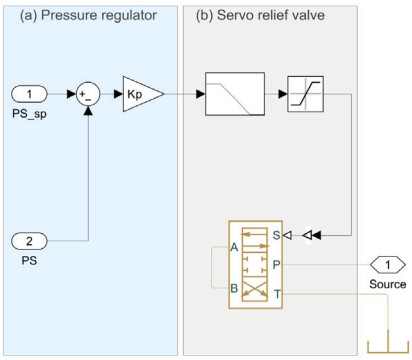

(b) Simscape scheme of of the supply pressure control realized by means of the servo-relief valve.

Fig. 8. Simscape diagrams.

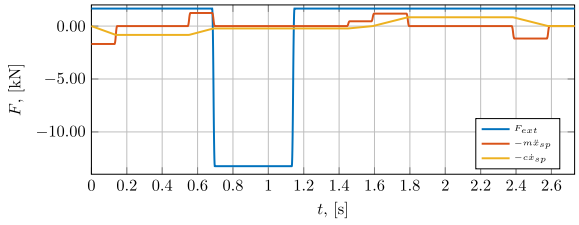

(a) HALE module inputs.

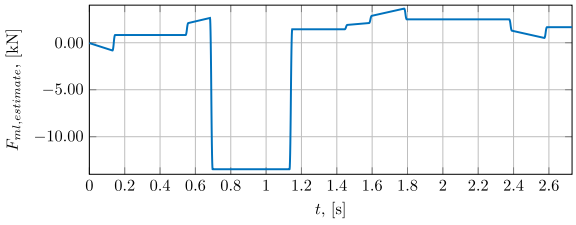

(b) HALE module output

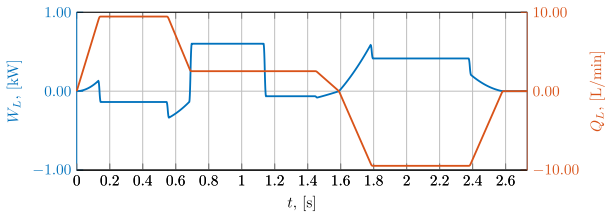

(c) HEO module inputs

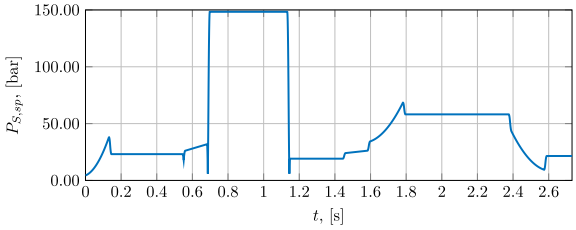

(d) HEO module output

Fig. 9. Inputs and outputs of the HALE and HEO modules for the blanking press cycle.

due to the high blanking forces. The pressure required during the fast approach is lower than that required during the return. This is due to the different role of the gravitational action, and also to the different velocities that occur in the two phases. In particular, from the comparison of Figs. 9(c) and 9(d) it can be seen that comparatively small differences in the absolute value of the nominal flow result in rather large differences in the generated supply pressure setpoint.

3.1.1. Servo-pump pressure regulation (SPPR)

In this section, the results concerning the behaviour of the system when the supply pressure is controlled by means of the Servo-Pump Pressure Regulation architecture are shown. The first two graphs reported in Fig. 10 concern on the one hand the supply pressure P_S and flow rate towards the actuator Q_S (Fig. 10(a)), on the other the motion control performance (Fig. 10(b)). As regards the supply pressure (Fig. 10(a)), two lines are drawn: the set-point value (dashed black) and the actual value (blue). The two lines (pressure set point and actual value) are practically coincident showing that the SPPR implementation of the CHPS and the relevant control system guarantee very high performances. Concerning on the other hand the flow rate Q_S, the nominal one (obtained as $Q_{S,sp} = A|\dot{x}_{sp}|$) is drawn as a dotted black line, whereas the actual one is represented in dark red. It can be seen that the actual flow Q_S generally follows the nominal one, except for the instants at which a sharp variation of the pressure P_S is observed. This effect can be attributed to the compressibility of the fluid taken into account in the simulation.

The graphs represented in Fig. 10(b) show that the position set-point is accurately followed. For the speed a higher following error occurs, as highlighted in the same plot. Some oscillations are present, mainly in the time span between 1.1 s and 1.6 s. This behaviour can be mainly ascribed to the HAR (hydraulic actuator regulator) chosen for this simulation. However, the goal of this simulation and of the following ones is not to optimize the performances of HAR, but to demonstrate the effectiveness of the new proposed methodology. Such oscillations do not significantly affect the required and wasted power and energy, and therefore neither the effectiveness of the methodology. Fig. 11(a) shows the graph of the actuator's servo-valve opening; being the servo-valve directly driven by the HAR, its opening has some oscillations too.

Finally, Fig. 11(b) shows on the one hand the energy entering the system and on the other the energy wasted across the actuator's servo-valve. It can be seen that the input energy is mainly wasted in the actuator's servo-valve. It may be noticed that until 0.7 s the input energy is lower than the energy wasted in the servo-valve; this is because in that time range the external force has a driving action, and so it introduces power in the system.

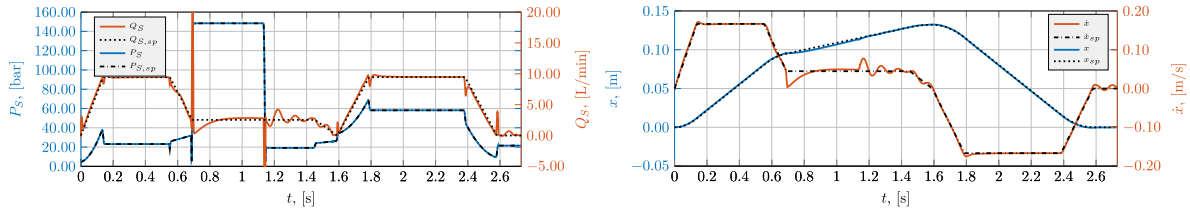

(a) Hydraulic Power Supply: set-point ($P_{S,sp}$) and actual (P_S) pressures; nominal ($Q_{S,sp}$) and actual (Q_S) flow rate.

(b) Position and velocity: set-points and actual values

Fig. 10. Blanking Press case study — SPPR: pressure regulation and close-loop motion profiles. (For interpretation of the references to colour in this figure legend, the reader is referred to the web version of this article.)

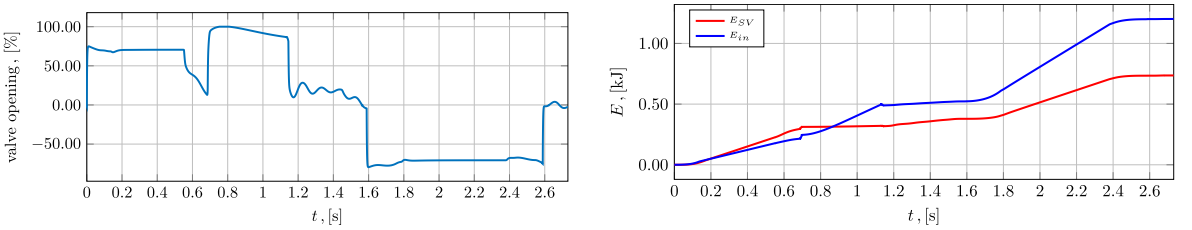

(a) Blanking Press case study - SPPR: servovalve percentage opening.

(b) Input hydraulic energy (E_{in}) and wasted energy across the actuator's servo-valve (E_{SV})

Fig. 11. Blanking Press case study — SPPR: servovalve opening (a) and energy consumption (b).

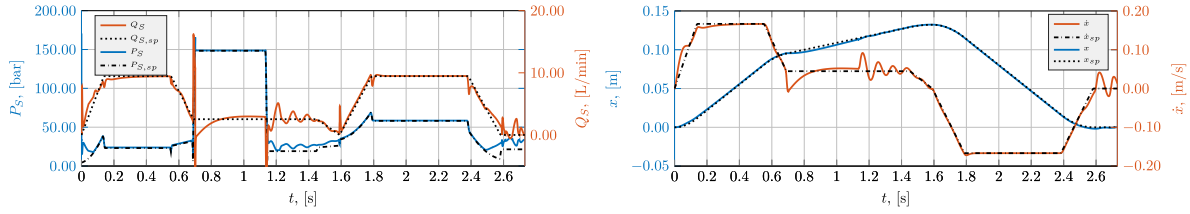

(a) Hydraulic Power Supply: set-point ($P_{S,sp}$) and actual (P_S) pressures; set-point ($Q_{S,sp}$) and actual (Q_S) flow rate.

(b) Position and velocity: setpoints and actual values

Fig. 12. Blanking Press case study — SVPR: pressure regulation and close-loop motion profiles.

3.1.2. Servo-relief valve pressure regulation (SVPR)

This section reports the results when the Servo-relief Valve Pressure Regulation (SVPR) architecture is applied. This case features a fixed displacement pump driven at constant speed, with a servo-valve used to regulate the supply pressure through the controlled discharge of the excess fluid. Fig. 12(a) shows that the flow rate Q_S behaves similarly to the previous case; however the supply pressure set-point is followed less accurately, mainly when the it sharply changes. In particular, at 0.7 s there is an additional negative peak of the servo-valve's flow-rate, and the servo-valve saturates keeping its opening at the maximum value for approximately 1.5 s (Fig. 14(a)). The servo-valve's saturation causes a position and speed following error higher than in the previous cases, as shown in Fig. 12(b). However, even if this is a non optimal behaviour, it does not significantly affect the comparison between the different architectures for supply pressure regulation, and the evaluation of power and energy required in the different cases.

Fig. 12(b) additionally shows that also for SVPR some speed oscillations occur, particularly between 1.1 s and 1.6 s. As already mentioned in the previous sections, they do not significantly affect the required and wasted energy.

Fig. 13 depicts the servo-relief valve opening (Fig. 13(a)) and the discharged flow-rate (Fig. 13(b)). The fact that a portion of the fluid is discharged towards the unpressurized tank introduces a relevant energy dissipation, that on the contrary does not occur in the previously analysed SPPR circuital solution. Consequently Fig. 14(b) displays not only the input hydraulic energy and the energy wasted across the actuator's servo-valve, but also the losses attributable to the servo-relief valve.

3.2. Die-casting case study

Die casting is a manufacturing process that can be used to produce pieces with high dimensional accuracy, a strong surface quality, and an almost perfect shape in a short time. High pressure is used to press molten metal, most frequently aluminium, into the cavity of a reusable steel mold (the die). The air is released through vents while the metal is forced through the feed system. The casting is released when the die halves have been separated (Dalquist & Gutowski, 2004). The total cycle time is very short, typically between 2 s and 1 min.

A die-casting process comprises four main phases, as described by Adamane et al. (2015):

- **hot sleeve filling**: the hot sleeve is filled with the molten metal, and the plunger moves at a slow speed to avoid turbulence;
- **filling of the die cavity**: filling of the die cavity at high velocity to avoid premature solidification at the gate and incomplete castings;
- **intensification phase**: application of high pressure to the molten metal as soon as the die cavity is full;
- **quick return**: at the end of the die-casting process a rapid repositioning is required.

Fig. 15 shows the inputs and outputs of the HALE and HEO modules; their final output is the supply pressure set point $P_{S,sp}$, represented in Fig. 15(d), which is directly passed to the controller connected to the CHPS module. As in the blanking case study, the HALE and HEO modules require a lumped-parameter model of the hydraulic actuator,

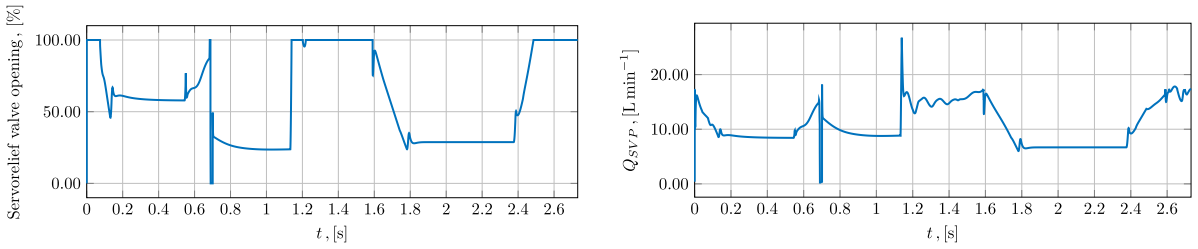

(a) Servo-relief valve opening

(b) Flow across the servo-relief valve

Fig. 13. Blanking Press case study — SVPR: servo-relief valve opening and discharged flow.

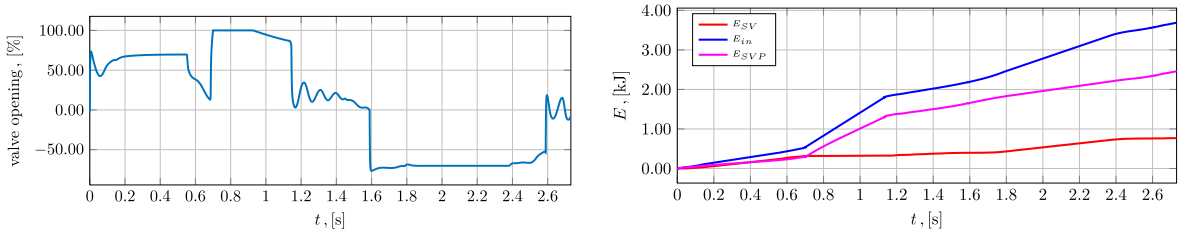

(a) Blanking Press case study - SVPR: Servovalve percentage opening.

(b) Blanking Press case study - SVPR: Input hydraulic energy (E_{in}), wasted energy across the actuator's servo-valve (E_{SV}), wasted energy across the servo-relief valve (E_{SVP})

Fig. 14. Blanking Press case study — SVPR: Valve opening and energy consumption.

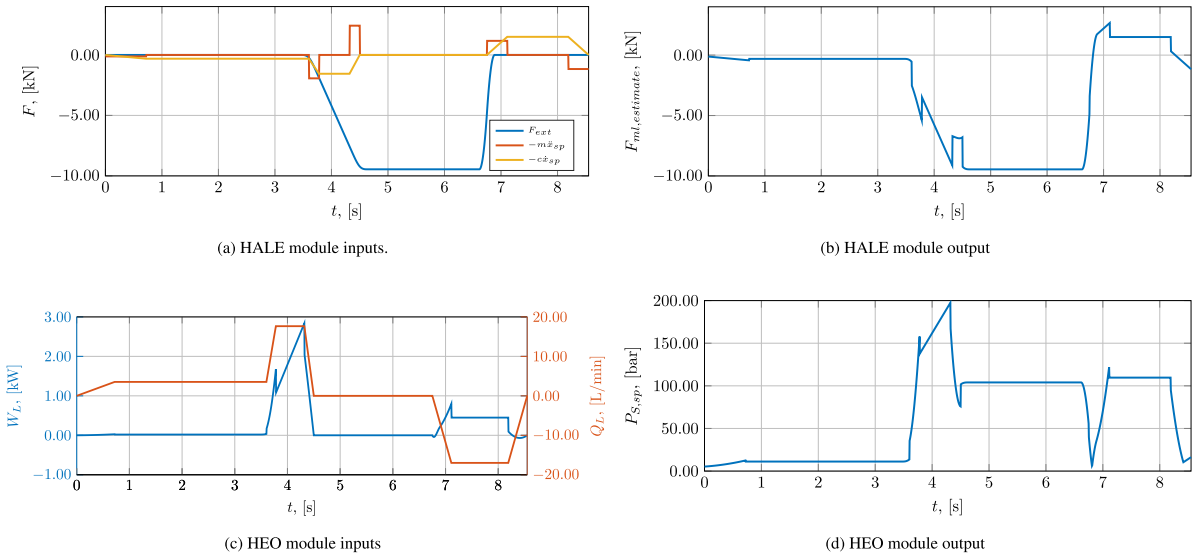

(a) HALE module inputs.

(b) HALE module output

(c) HEO module inputs

(d) HEO module output

Fig. 15. Die-Casting case study: inputs and outputs of the HALE and HEO modules.

the velocity and acceleration setpoints, and an estimate of the external forces.

The output of the HALE module, shown in Fig. 15(b), identifies a low mechanical load on the actuator for the first 3 s; thereafter, the load increases according to the increase in the external force required for the application. Fig. 15(d) shows the supply pressure as output of the HEO module; the required supply pressure is low in the first 3.5 s; at this time, the supply pressure suddenly increases towards 200 bar, while it remains close to 100 bar in the following time. It is interesting to note that the peak pressure is not required during the intensification phase, but during the filling of the die cavity. This is because the latter occurs at high velocities and flow rates, which require high pressure due to the dissipation occurring in the servo-valve. The intensification phase, on the other hand, is purely static. Even during the quick return phase, there is a relevant pressure requirement due to the velocity that the piston must reach. The main effect of the velocity is not directly related to the frictional forces, but to the flow through the servo-valve, with the associated pressure drop.

In the following, the results regarding the die-casting study case are reported.

3.2.1. Servo-pump pressure regulation

Figs. 16 and 17 show the results of the simulation for the Die-casting case study with SPPR. The supply pressure set-point (Fig. 16(a)) is constant and very low between 0.5 and 3.5 s, consistently with the hot sleeve filling at constant speed and only with viscous resistance. During the rapid filling of the cavity significant inertia actions arise and subsequently in the intensification phase a high pressure is required. This justifies the trend of the pressure reference between about 3.5 and 7 s. In the final phase of the cycle, the actions of inertia and the viscous resistance, which changes sign coherently with the speed, have a significant effect. Due to the compressibility of the hydraulic fluid, the sharp variations of pressure have an effect on the actual

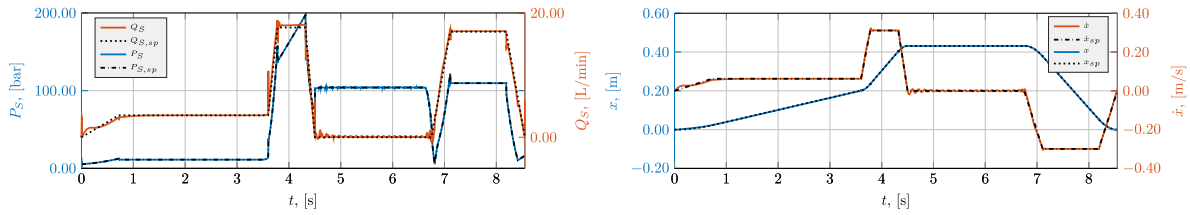

(a) Hydraulic Power Supply: set-point ($P_{S,sp}$) and actual (P_S) pressures; set-point ($Q_{S,sp}$) and actual (Q_S) flow rate.

(b) Position and velocity: set-points and actual values

Fig. 16. Die-Casting case study — SPPR: pressure regulation and close-loop motion profiles.

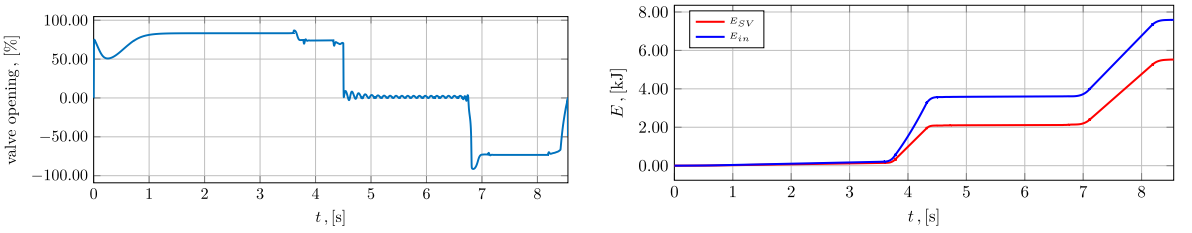

(a) Die-Casting Press case study - SPPR: servovalve percentage opening.

(b) Input hydraulic energy (E_{in}) and wasted energy across the actuator's servo-valve (E_{SV})

Fig. 17. Die-Casting case study — SPPR: servovalve opening (a) and energy consumption (b).

flow rate Q_S, which correspondingly shows sharp peaks. These peaks do not affect the piston's speed; less pronounced and lower frequency deviations from the nominally required $Q_{S,sp}$ can on the other hand be attributed to the control system, and are clearly reflected also in the piston actual velocity (Fig. 16(b)). The closed-loop position and speed motion laws, represented in Fig. 16(b), are well followed. Small amplitude oscillations are detectable in the speed behaviour, especially during the intensification phase, and very small overshoots at the end of the acceleration and deceleration phases occur. These phenomena are of very limited amplitude and a finer tuning of the control parameters could lead to their further reduction.

The trend of the opening percentage of the servo-valve (Fig. 17(a)) which controls the fluid directed to the actuator does not present particular critical issues and is compatible with the dynamic performance of this type of valve. Between about 4.5 s and 6.8 s oscillations around the valve's null point can be seen; the amplitude of this oscillation is limited and the frequency is not critical. As shown in Fig. 17(b), the most energy consuming phase of the process is the die cavity filling phase, followed by the quick return. The servo valve losses are the main cause of energy consumption of the system. Unlike the blanking press case, the external actions are always passive and the input energy is always higher than the energy losses in the servo-valve.

3.2.2. Servo-relief valve pressure regulation

By applying the SVPR power supply in simulation, the results shown in Figs. 18 to 20 are obtained.

Fig. 18(a) shows that in the initial cycle phase (the hot sleeve filling) the supply pressure does not follow the reference, but settles at a higher value. This is due to the opening of the servo-relief valve reaching saturation, as can be observed in Fig. 19(a). Being at the maximum opening, and not being able to open further, it is not possible to obtain an inlet pressure which allows to correctly follow the pressure reference. This translates into higher energy consumption in this phase compared to the previous case, as shown in Fig. 20(b).

Compared to the case using the SPPR architectures, also the degree of opening of the actuator servo-valve in this initial phase of the cycle is different, as evident in Fig. 20(a), while a similar trend is observed for the other phases.

Also the dynamics of the system in the initial phase of the cycle is more unstable, with oscillations of the piston velocity (apparent in Fig. 18(b)) that did not occur in the previous case.

Fig. 20(b) shows the energy consumption with the SVPR power supply. It is evident that in the first and third phases the dissipation in the servo-relief valve represents the prevailing term, while in the second and fourth phases, where speeds and so flow-rates increase, losses in the servo-valve increase as well, becoming significant with respect to phases one and three.

3.3. Deep drawing press case study

Deep drawing is a technological process for forming a flat metal sheet, by pressing it in a die, without causing breakage or excessive localized thinning. The deep drawing process begins by pressing a metal blank into a cavity, that draws the blank into the desired shape. The final deep-drawn component must maintain its integrity and strength, so the process is carried out in small, progressive steps to ensure an even distribution of metal across the final mould. Deep drawing is widely used in the industry, to produce e.g. beverage and food cans, kitchen sinks, cookware, engine oil pans, solenoid assemblies, and automotive fuel tanks.

The deep drawing process includes three main phases:

- **fast approaching**: phase of rapid approach to the workpiece, in which the rod performs part of the downward stroke without resistance;
- **drawing phase**: when the blank is encountered, the drawing process begins and a constant resistance is experienced;
- **fast returning**: fast return to the bottom dead centre.

The results of the case study on the drawing press are reported below. Similarly to the previously considered case studies, the inputs and outputs of the HALE and HEO modules are shown in Fig. 21. The inputs required for the two modules are: the motion profile setpoints up to the accelerations, a lumped-parameter model of the hydraulic actuator, and an estimation of the external forces. Their final output is the supply pressure setpoint $P_{S,sp}$. As can be seen in Fig. 21(a) the main force is the external force, which is composed of a gravitational term, which is clearly visible during the initial rapid approaching and the final quick return phases, and a drawing force term, which is evident during the intermediate interval of the work cycle. The friction and inertial forces, on the other hand, are of a lower order of magnitude. The output of the HALE module, which is in Fig. 21(b), clearly reflects these contributions. Concerning the HEO module inputs, shown in

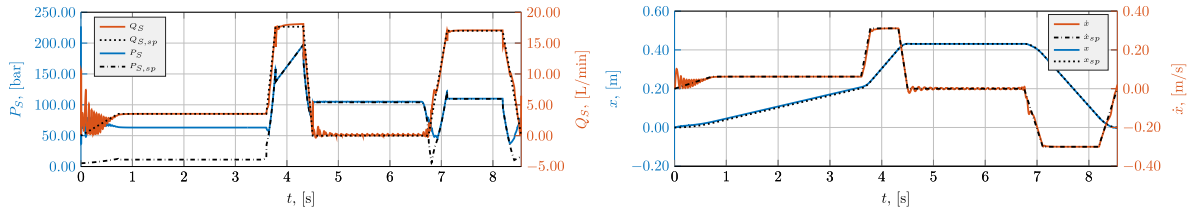

(a) Hydraulic Power Supply: set-point ($P_{S,sp}$) and actual (P_S) pressures; set-point ($Q_{S,sp}$) and actual (Q_S) flow rate.

(b) Position and velocity: setpoints and actual values

Fig. 18. Die-Casting case study — SVPR: pressure regulation and close-loop motion profiles.

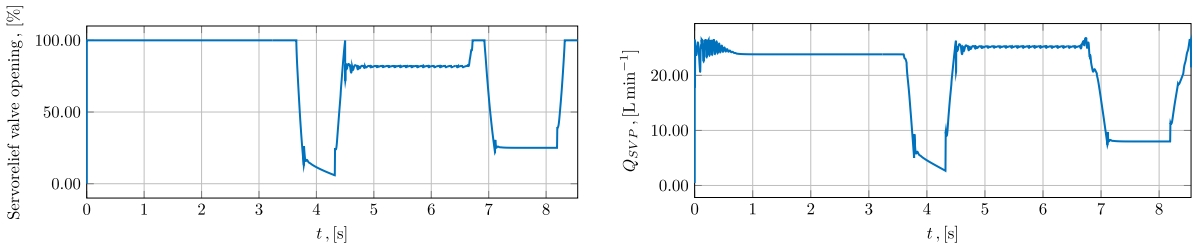

(a) Servo-relief valve opening

(b) Flow across the servo-relief valve

Fig. 19. Die-Casting Press case study — SVPR: servo-relief valve opening and discharged flow.

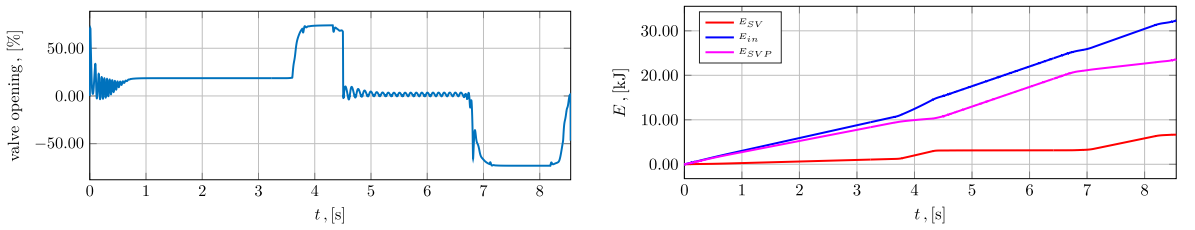

(a) Die-Casting case study - SVPR: Servovalve percentage opening.

(b) Die-Casting case study - SVPR: Input hydraulic energy (E_{in}), wasted energy across the actuator's servo-valve (E_{SV}), wasted energy across the servo-relief valve (E_{SVP})

Fig. 20. Die-Casting case study — SVPR: Valve opening and energy consumption.

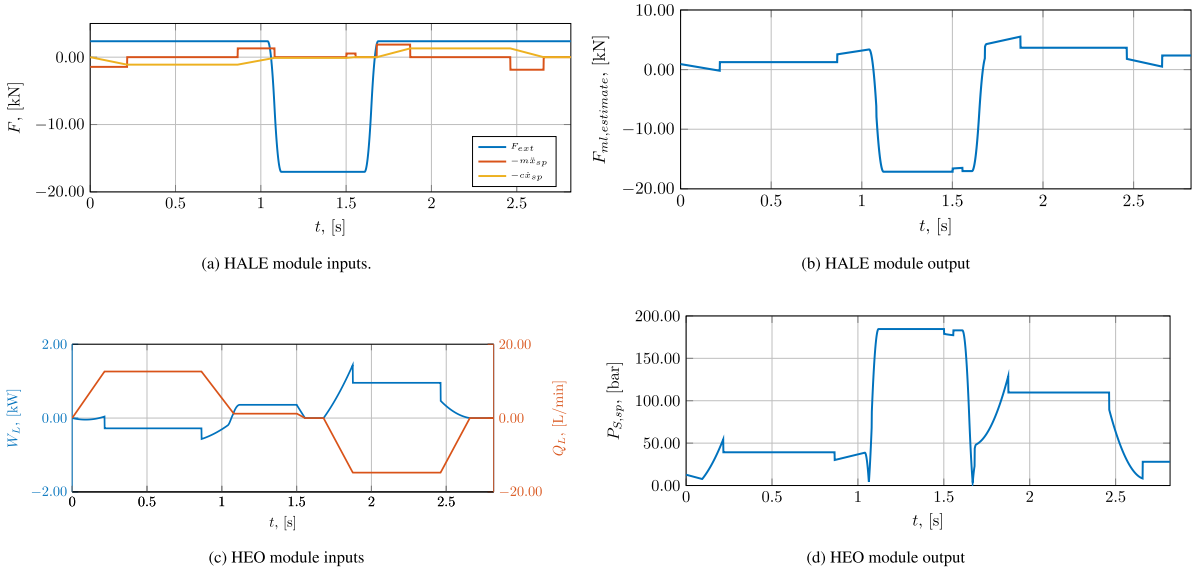

(a) HALE module inputs.

(b) HALE module output

(c) HEO module inputs

(d) HEO module output

Fig. 21. Drawing press case study: inputs and outputs of the HALE and HEO modules.

Fig. 21(c), it can be seen that the power W_L changes sign repeatedly during the work cycle, due to the effects of gravity (which adds energy to the system during the fast approach phase) and of the other forces. The generated $P_{S,sp}$, reported in Fig. 21(d) clearly shows the influence

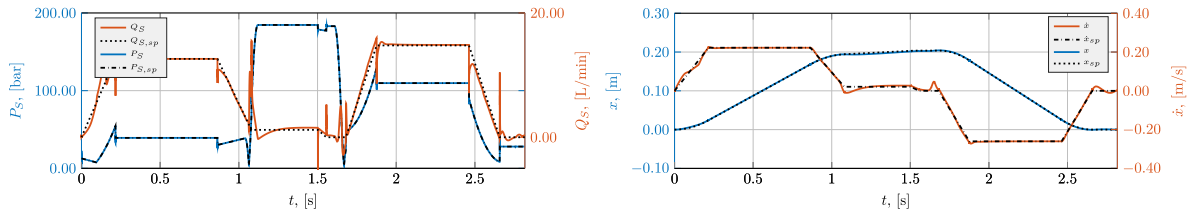

(a) Hydraulic Power Supply: set-point ($P_{S,sp}$) and actual (P_S) pressures; set-point ($Q_{S,sp}$) and actual (Q_S) flow rate.

(b) Position and velocity: set-points and actual values

Fig. 22. Drawing press case study — SPPR: pressure regulation and close-loop motion profiles.

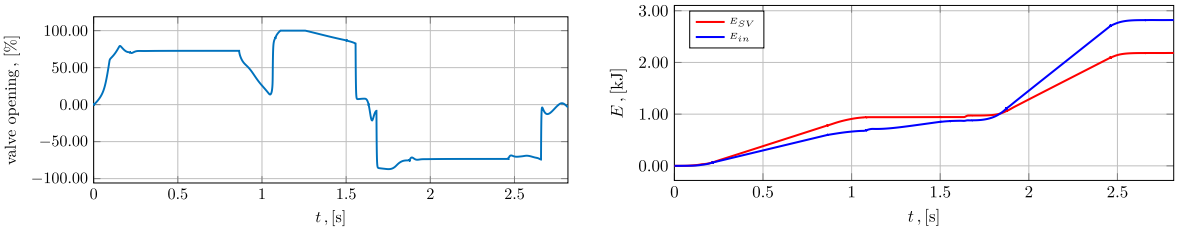

(a) Drawing Press case study - SPPR: servovalve percentage opening.

(b) Input hydraulic energy (E_{in}) and wasted energy across the actuator's servo-valve (E_{SV})

Fig. 23. Drawing press case study — SPPR: servovalve opening (a) and energy consumption (b).

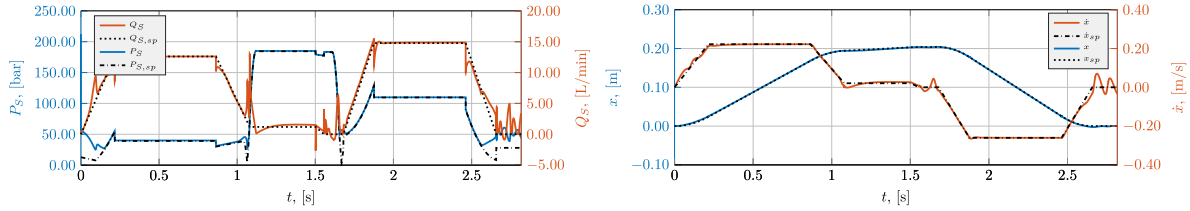

(a) Hydraulic Power Supply: set-point ($P_{S,sp}$) and actual (P_S) pressures; set-point ($Q_{S,sp}$) and actual (Q_S) flow rate.

(b) Position and velocity: setpoints and actual values

Fig. 24. Drawing press case study — SVPR: pressure regulation and close-loop motion profiles.

of the drawing force, which determines the maximum value of the required pressure. Notably, the role of gravity cannot explain the rather pronounced asymmetry that occurs in $P_{S,sp}$ during the approach and return phases. Rather, the difference is mainly due to the differences in the absolute value of Q_L.

3.3.1. Servo-pump pressure regulation

The graphs represented in Fig. 22(a) show that the actual supply pressure curve is practically coincident with the set-point. As for the working cycles of the other case studies, it shows that SPPR and the relevant control system guarantee very high performances in terms of pressure regulation. Concerning the flow towards the actuator Q_S, it can be seen that sharp deviations from the nominal $Q_{S,sp}$ occur together with sudden pressure variations; they do not appear however to significantly affect the actual speed of the piston, represented in Fig. 22(b). The same figure shows a position following error between approximately 1.1 s and 1.6 s mainly caused by the servo-valve saturation that occurs at 1.1 s (see Fig. 23(a)). As a consequence, a following error is present also for the speed. As previously said, this does not significantly affect the energy requirements and consumption.

The energy quantities related to this case study are depicted in Fig. 23(b). Similarly to the blanking case study, there is an initial time range where the input energy provided by the pressure supply is lower than the energy wasted in the servo-valve. This time range corresponds to the fast approach phase in which the piston performs a descent stroke and has no resistant force applied. In this phase, energy is introduced in the system by the gravitational force.

3.3.2. Servo-relief valve pressure regulation

The results obtained by the application of the SVPR power supply are overall similar to the ones obtained with the other architecture. Concerning the control of the supply pressure P_S, in Fig. 24(a) it can be seen that the setpoint is well followed except for the time intervals in which the servo-relief valve opening (represented in Fig. 25(a)) reaches full saturation. The flow towards the actuator Q_S, also depicted in Fig. 24(a), shows as in the other case studies sharp peaks corresponding to sudden variations of the supply pressure. Also the flow across the servo-relief valve, displayed in Fig. 25(b), shows these characteristic peaks. The actual position of the piston follows accurately the setpoint, as shown in Fig. 24(b), whereas the velocity shows some oscillations towards the end of the cycle, despite the fact that the actuator servo-valve does not reach saturation (Fig. 26(a)). Concerning energy consumption (Fig. 26(b)) it can be highlighted that the main energy losses occur across the servo-relief valve, with smaller energy dissipation also on the actuator's servo-valve.

4. Discussion

This section discusses the results obtained by applying the proposed methodology to the three industrial cases. The discussion of the methodology does not focus on the typology of the controllers needed to control the actuator's position and the hydraulic power supply. Instead, it considers the energy savings that can be achieved depending on the type of adjustable power supply used in the simulated

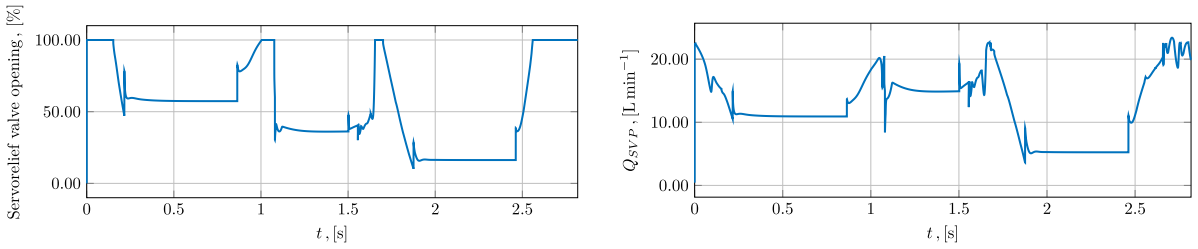

(a) Servo-relief valve opening

(b) Flow across the servo-relief valve

Fig. 25. Drawing Press case study — SVPR: servo-relief valve opening and discharged flow.

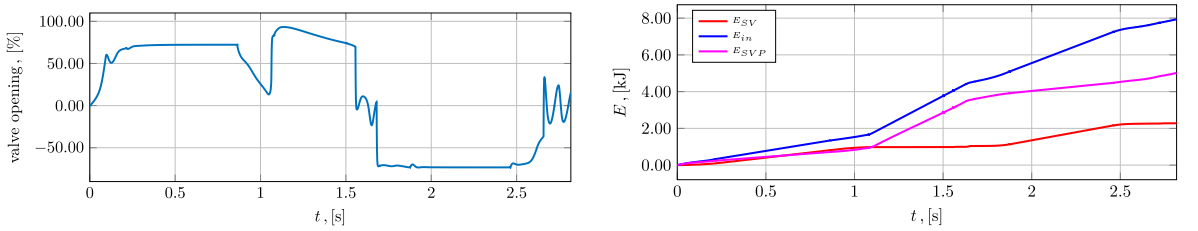

(a) Drawing press case study - SVPR: Servovalve percentage opening.

(b) Drawing press case study - SVPR: Input hydraulic energy (E_{in}), wasted energy across the actuator's servo-valve (E_{SV}), wasted energy across the servo-relief valve (E_{SVP})

Fig. 26. Drawing press case study — SVPR: Valve opening and energy consumption.

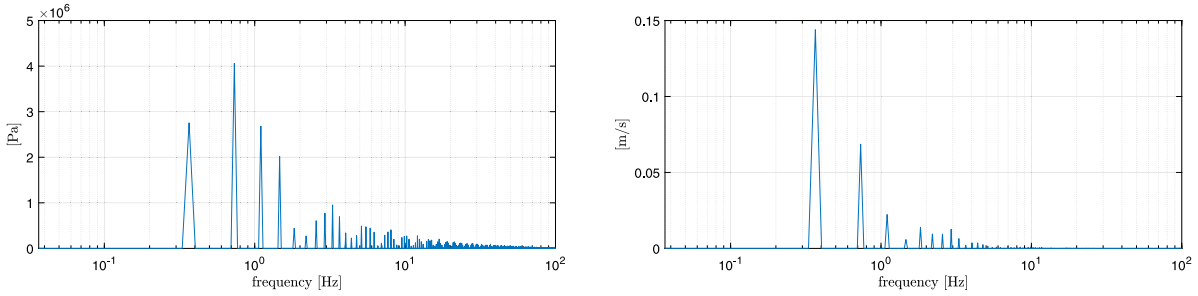

(a) Supply pressure set-point frequency spectrum

(b) Actuator's speed set-point frequency spectrum

Fig. 27. Blanking Press case study: set-points' frequency spectra.

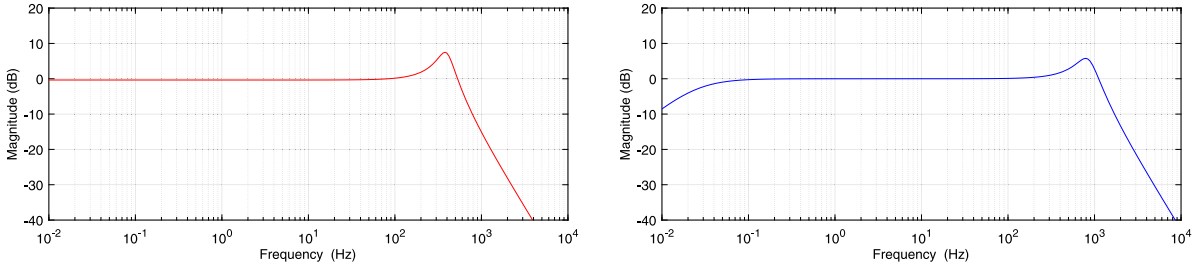

(a) Actuator's speed transfer function

(b) Supply pressure transfer function

Fig. 28. Closed-loop transfer functions.

application cases using a suitable controller for both the actuator and the hydraulic power supply.

The implementation of the methodology requires two controllers, one dedicated to the motion of the actuator and one for the control of the hydraulic supply source. The simulations presented in the previous sections use two simple regulators, a PD regulator as the actuator position controller and a P regulator for controlling the hydraulic supply source. The parameters of both controllers were set to fulfil the time characteristics of the position and pressure setpoints. For instance, Fig. 27 shows the frequency spectrum of the position and pressure setpoints used in the simulation for the Blanking machinery using the SVPR power supply architecture. Fig. 28(a) depicts the magnitude Bode plot of the transfer function between the actuator's law of motion setpoint and the actual speed for the SVPR architecture evaluated at constant supply pressure and constant external force.

For the same three application cases, the effectiveness of the proposed methodology is tested using two different Controlled Hydraulic Power Supply: the first is based on a Servo-Pump Pressure Regulation and the second on a Servo-relief Valve Pressure Regulation. The evaluation of the methodology does not consider other commercially

Table 4
CFCP architecture operating parameters (pump pressure P_S and pump flow rate Q_P) for each case study.

	Blanking	Die Casting	Drawing
$P_{S,CFCP}$, [bar]	171	227	212
$Q_{P,CFCP}$, [L/min]	10.7	19.3	15.1

Table 5
Motor/driver efficiencies for the different AHPS.

AHPS	Motor/driver	Efficiency
CFCP	asynchronous motor + inverter	88%
SPPR	brushless servomotor + driver	96%
SVPR	asynchronous motor + inverter	88%

available controlled hydraulic power supplies discussed in paragraph 2.3 because of their small bandwidth with respect to the dynamic behaviour required for the application cases. Moreover, the methodology uses the same Hydraulic Efficiency Optimizer for all the simulated cases according to the model proposed in paragraph 3.

4.1. Energy consumption comparison

In this section the simulation results are compared in terms of energy consumption. The comparison focuses in particular on the input energy required by the system for the three case studies, as the controlled hydraulic power supply varies.

The considered industrial applications often use a constant pressure and constant flow power supply in conjunction with a relief valve that discharges the excess flow rate, implementing the classic architecture with FD pump, FS electric drive. This architecture is a non-adjustable power generation system and denoted as CFCP. It generates a constant pressure, does not satisfy the requirements of the proposed methodology and, under these conditions, the system has the maximum energy waste. The difference between the installed power and the demanded power during the cycle is dissipated in the circuit, where pressure drops occur (in the pressure relief valve and in the proportional directional valve). The costs, both for the pump and for the electric drive, are lower than the ones for solutions with the possibility of regulating the fluid power. This section uses the energy demand of this common architecture as a first benchmark for the energy saving achievable with the proposed methodology. The operating parameters (namely the hydraulic power supply operating pressure P_S and generated flow rate Q_P) of the CFCP architecture that are considered for the benchmark are reported for the three case studies in Table 4. These values were selected taking into account a slight increase in the peak requirements of each application. These requests relate to the peak flow rate towards the actuator and the peak pressure. As a result for all three cases the CFCP solution is characterized by $Q_{P,CFCP} > \max(|Q_{S,sp}|)$ and $P_{S,CFCP} > \max(P_{S,sp})$. On the other hand, the energy demand of the identical systems equipped with the IPS is considered as a second benchmark to highlight the maximum theoretical energy savings obtainable with the proposed methodology.

In addition to the energy wasted via the components downstream of the pump, the simulation results also takes into account the energy wasted in the pump, the electric motor, and the relevant driver, according to the different hydraulic power supplies used.

Table 5 summarizes the values of the efficiencies considered for motors and drivers. Of course, for IPS the overall efficiency of the pump, motor and driver is considered unitary, being an ideal case.

The graphs of input power and input energy obtained by the methodology with the IPS, SPPR and SVPR controlled hydraulic power supplies are depicted in Figs. 29, 30 and 31 respectively for the Blanking, Die-casting and Deep Drawing processes. The graphs for the CFCP architecture (dotted grey line) are also reported. The high energy consumption of the CFCP architecture results from the constant supply

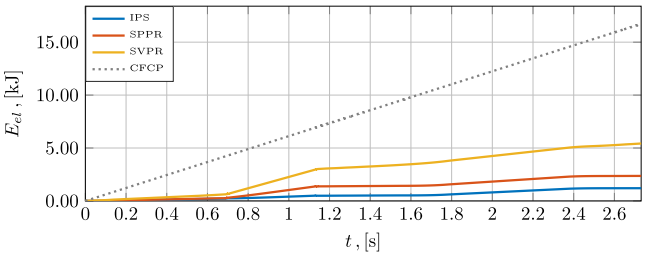

Fig. 29. Blanking Press case study: comparison of energy consumption resulting from different power supply architectures.

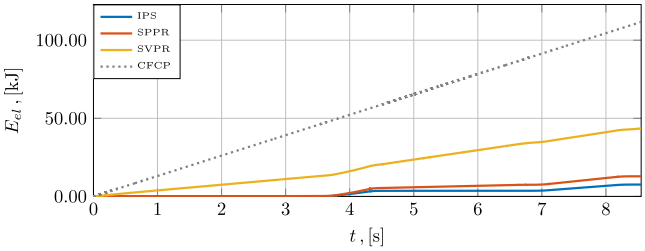

Fig. 30. Die-Casting case study: comparison of energy consumption resulting from different power supply architectures.

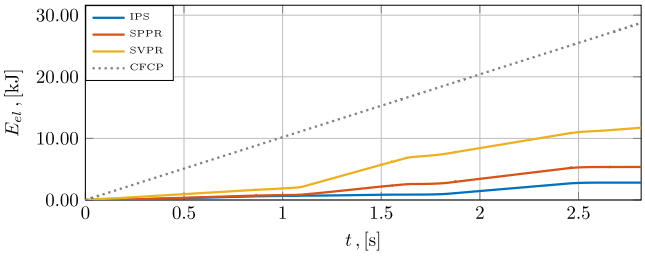

Fig. 31. Drawing Press case study: comparison of energy consumption resulting from different power supply architectures.

pressure and flow rate of the pump, which must be slightly higher than the relevant peak values reached during the work cycle. This method wastes a lot of energy across the relief valve, and has an input power that is much higher than the one needed by the load and the one wasted across the actuator's servo-valve. As already mentioned, the estimated input power also includes the efficiency of the pump and the asynchronous motor that drives the pump and the associated inverter (see Table 5).

Figs. 29–31 show that for each considered case study, the methodology using the IPS requires the lowest values of input energy. In this case, the power source has unity efficiency, and the energy wasted via the actuator's servo-valve is the only additional input energy required.

Input energy and power increase if the methodology uses SPPR since additional power and energy are wasted on the servo-motor, the associated drive system and the pump. The overall efficiency of brushless servo-drives is very high and, despite its dependence on the motor speed, an average value of 96%, as shown in Table 5, is appropriate for the size of the electric drive system considered in the simulations.

The methodology using a SVPR controlled hydraulic power supply exhibits a further increase in wasted energy. In this case, the losses in the asynchronous motor, pump and servo-relief valve are added to the energy dissipated in the servo-valve. An IE3 asynchronous motor of the size considered in the simulations (between 5 and 10 kW) has an efficiency of around 90% at the nominal speed. Overall, the efficiency at the level of electrical actuation is worse than in the case of the SPPR power supply.

Table 6
Energy costs per cycle, [kJ].

	Supply architecture/using methodology			
Case study	IPS/yes	SPPR/yes	SVPR/yes	CFCP/no
Drawing	2.8	5.4	11.7	28.7
Blanking	1.2	2.4	5.4	16.7
Die Casting	7.6	12.9	43.5	111.7

Table 7
Process data for the three case studies. t_c = cycle time; c_h = cycle/hour; h_d = hours/day; d_y = days/year.

Case study	t_c [s]	c_h	h_d	d_y
Drawing	2.82	1276.60	16	250
Blanking	2.73	1318.68	16	250
Die Casting	8.55	421.05	16	250

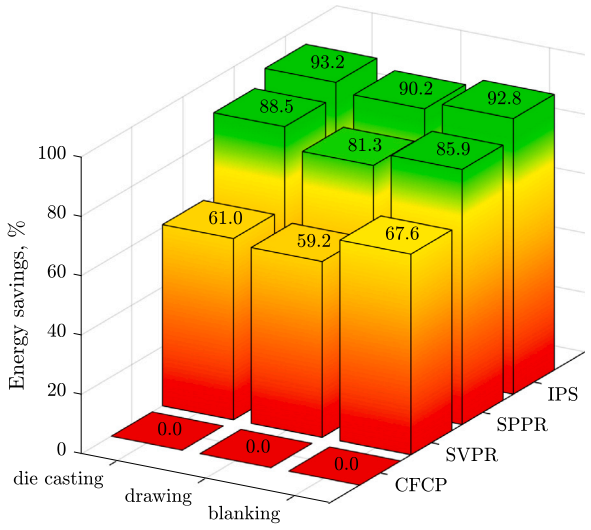

Fig. 32. Energy savings obtained for each work cycle using different power regulation strategies.

Finally, the hydraulic circuits that rely on the CFCP hydraulic power supply show the worst behaviour in terms of energy consumption; the energy requirements of this solution is more than twice as high as that of the SVPR architecture in all three case studies.

Fig. 32 summarizes the energy savings for the three application cases obtained by applying the proposed methodology with the controlled power supply IPS, SPPR and SVPR compared to the energy consumed by the same systems without the proposed methodology and using the CFCP architecture (E_{CFCP}). In particular, e.g. for SVPR architecture, the energy saving is evaluated as $(E_{CFCP} - E_{SVPR})/E_{CFCP}$, expressed as a percentage (where E_{SVPR} is the energy consumed by SVPR), using the values from Table 6. It shows that the energy saving decreases from IPS to SVPR, with the worst case energy saving being more than 59%.

In the Drawing and Blanking cases, the savings are almost comparable to SPPR, while a slightly higher saving is achieved with SVPR for Blanking. For the Die Casting process, the percentage saving is quite higher, for SPPR and IPS architectures, than that obtained for the other two cases. For the Blanking and Drawing cases the cycle time (Table 7) is quite similar, about 2.6 s, for Die Casting it is more than 8 s. Therefore, in the Die Casting case higher savings may be due to the longer cycle time with a significant load fluctuation in the cycle.

The results shown and tabulated here demonstrate the high efficiency gains that can be achieved thanks to the proposed methodology. However, further improvements may be obtained through more advanced techniques for the implementation of the HEO module, which could be based on optimization methods that are beyond the scope of this work. As mentioned earlier, the proposed HEO module relies instead on a fixed value of H^*; however, even with this simple solution the choice of H^* should be performed with some care. Fig. 33 reports the results of a sensitivity analysis performed for the drawing press case study. For each simulation run, the value of the HEO parameter H^* was set to a value in the range $[0.5, 1]$. The parameters of the control systems were left unchanged. Fig. 33(a) shows the dependency between energy consumption over an entire work cycle and H^*. It is clear that higher values of H^* lead to considerable energy savings, and thus confirms the intuition suggested by Eq. (15). On the other hand, it can be seen in Fig. 33(b) that at higher values of H^* the actuator's servo-valve shifts its typical opening towards higher values, and may reach its saturation region, which should be avoided in order to maintain high motion control performance. In particular, for the case under study, saturation is reached when a value of $H^* = 0.85$ or greater is considered.

5. Conclusions

The paper presents a new methodology for increasing the efficiency of applications that use a hydraulic servo axis. The methodology consists of three modules, the Hydraulic Actuator Load Estimator, the Hydraulic Efficiency Optimizer and a Controlled Hydraulic Power Supply, leading to a system controlled by two parallel closed loops, one for the motion control of the hydraulic servo axis and one for controlling the hydraulic power supply. The control of the servo axis position is demanded to a servo-valve, whose circuital position remains unaltered with respect to the usual hydraulic servo-axis configuration; however, as a direct consequence of the proposed methodology, its operating point is shifted towards a condition of high opening, which in turn reduces throttling losses. This development is made possible by the introduction of the CHPS subsystem, which provides a controlled pressure supply based on the pressure set-point generated by the cascade processing of the two algorithm-based blocks HALE and HEO.

The paper discusses the methodology's modules both at the theoretical and at the application level. At the theoretical level, all modules are discussed in detail, and some possible approaches to optimizing their performance are presented. For the HEO module the paper proposes a direct, simple algorithm for determining the pressure setpoint for the CHPS based on characteristic equations of the servo valve. In addition, the paper discusses the controllable hydraulic power supplies that the proposed methodology can use, focusing on dynamic performances.

Without loss of generality of the methodology, the paper presents, at the application level, three validation cases based on industrial applications whose simulation results show that the methodology can lead to energy savings between 59% to 85% compared to the traditional CFCP architecture solution for hydraulic servo axes. These energy savings also significantly reduce the CO_2 emissions, estimated at 29.8 and 10.15 tons per year, respectively, in the best and worst case. The effective energy saving discussed in this paper depends on the characteristics of the controlled power supply used. This fact is emphasized by the introduction of two different high dynamics Controlled Hydraulic Power Supply suitable for the application of the methodology, the SPPR and the SVPR. While the highest energy savings were achieved with the CHPS based on the servo pump, the architecture based on the Servo-relief Valve Pressure Regulation for the presented industrial application still offers energy savings ranging from 59% to 61%. Importantly, the latter architecture has low implementation costs, as it can be obtained

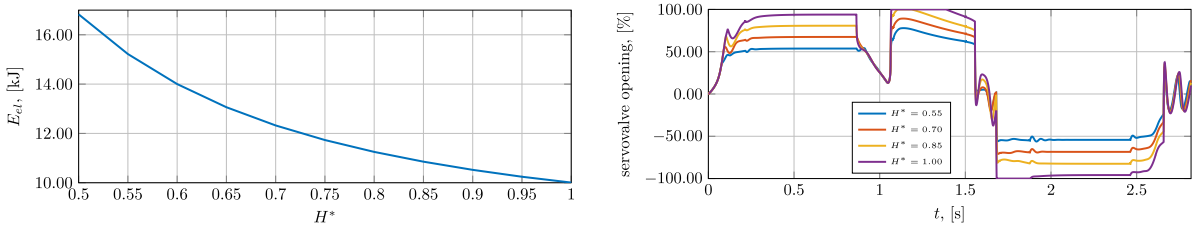

(a) Energy consumption at different values of H^*.

(b) Servo-valve opening at different values of H^*.

Fig. 33. Drawing press case study, SVPR Effects of H^* on energy consumption and servo-valve opening.

by simply installing a high dynamic servo-valve on existing CFCP systems.

Some synthetic references to the results available in the literature, and discussed in the introduction, in relation to similar application cases are reported below, in order to compare them with the results shown in this paper. An optimized design procedure for power supplies constituted by multiple motor-pumps presented by Huang et al. (2019) was applied to a 2000-ton rapid sheet tension hydraulic press, resulting in a 41.72% reduction in installed power and a 26.97% reduction in energy consumption. In the solution proposed by Li et al. (2017) the drive system is shared at different times by two hydraulic presses, which are combined so that the excessive energy of one can be utilized by the other, by adjusting its work cycle to coordinate the forming process. The method, when applied to two identical hydraulic presses with the nominal force of 20 MN in a tandem line, yielded electrical energy savings of 36%. An overall energy saving of the same order of magnitude as the previous ones, i.e. 20%, was achieved by Dindorf and Wos (2020) in his study on a hydraulic 80 MN forging press with parallel connection of three pumps and a real-time model predictive control based on multiple inputs multiple outputs, as well as a global predictive control.

In these works, the energy savings are obtained at the expense of increasing the number of motors and pumps (Huang et al., 2019), by carefully modifying and combining the working cycles of two different presses (Li et al., 2017), or by introducing several circuital modifications (Dindorf & Wos, 2020).

The methodology here described, on the other hand, does not require any significant alterations to either the hydraulic circuit or the executed work cycle; at the same time, the obtained energy savings correspond to or even exceed those described in the literature. Indeed, a remarkable feature of the proposed methodology is its generality and its low complexity in terms of system architecture. The methodology is not customized to solve a specific problem or to be applied in a specific domain and, moreover, it can be easily implemented in any existing system without the need to fundamentally change its configuration.

Moreover, the controlled hydraulic power supply presented in this paper makes the methodology applicable to cases where the bandwidth of the control signal (position and pressure) is high. This choice also introduces a new control scheme for motion control with a hydraulic actuator, based on the regulation of both the hydraulic power supply and the servo-valve of the actuator.

The presented methodology can be applied to a wide range of application fields. The three discussed in the paper are only examples where the dynamic of the system is high. Similarly, the methodology can be applied to systems with lower dynamics, allowing the use of adjustable hydraulic power supplies with narrower bandwidths.

The methodology can lead to high energy savings, in any of its implementations, even with simple approaches for the HALE and HEO modules, as presented in this article. Moreover, the application cases' simulations show that the proposed methodology can be successfully applied to industrial cases, using a simple and cheap controlled hydraulic power supply such as that of SVPR.

The authors are planning the next step to validate the methodology from an experimental perspective. The experimental validation requires the implementation of the three modules that make up the methodology. The simulation results show that the realization of the CHPS module using the SVPR architecture is quite simple and physically feasible. Moreover, the hydraulic circuit is very similar to those used in the usual hydraulic servo-axis solutions. Similarly, the simulations show that the experimental realization of the HALE module is possible with the same approach presented in the simulation sections, based on the knowledge of the kinematic state of the actuator, some mechanical parameters of the actuator and the working force required for application. The software implementation of this module is simple since the application force is known as a function of the position of the actuator, as is common in industrial applications with fixed cycles. The experimental implementation of the HEO module presents no difficulties when its configuration corresponds to that presented in the simulations. In other cases, the definition of the complexity of the module requires additional investigation.

Acronyms

AHPS	Adjustable Hydraulic Power Supply.
APV	Actuator Proportional Valve.
CFCP	Constant Flow Constant Pressure.
CHPS	Controlled Hydraulic Power Supply.
DDH	Direct Driven Hydraulics.
EDC	Electric Drive Cost.
EHA	Electro-Hydraulic Actuator.
FD	Fixed Displacement.
FS	Fixed Speed.
HALE	Hydraulic Actuator Load Estimator.
HAR	Hydraulic Actuator Regulator.
HEO	Hydraulic Efficiency Optimizer.
HPS	Hydraulic Power Supply.
HPSR	Hydraulic Power Supply Regulator.
HSA	Hydraulic Servo Actuator.
IPS	Ideal Pressure Source.
MPG	Motion Profile Generator.
PCD	Pump Control Dynamics.
PPRV	Proportional Pressure-Relief Valve.
PRV	Proportional Relief Valve.
SCD	System Control Dynamics.
SMISMO	Separate Meter-In Separate Meter-Out.
SPPR	Servo-Pump Pressure Regulation.
SRV	Servo-Relief Valve.
SVPR	Servo-relief Valve Pressure Regulation.
VD	Variable Displacement.
VDC	Virtual Decomposition Control.
VDFS	Variable Displacement Fixed Speed.
VDSP	Variable Displacement Servo-Pump.
VS	Variable Speed.

Declaration of competing interest

The authors declare that they have no known competing financial interests or personal relationships that could have appeared to influence the work reported in this paper.

References

Aboelela, M. A., Essa, M. E. -S. M., & Hassan, M. M. (2018). Modeling and identification of hydraulic servo systems. *International Journal of Modelling and Simulation*, *38*, 139–149.

Adamane, A. R., Arnberg, L., Fiorese, E., Timelli, G., & Bonollo, F. (2015). Influence of injection parameters on the porosity and tensile properties of high-pressure die cast Al-Si alloys: A review. *International Journal of Metalcasting*, *9*, 43–53.

Ahmadi, K., Asadi, D., Merheb, A., Nabavi-Chashmi, S. -Y., & Tutsoy, O. (2023). Active fault-tolerant control of quadrotor UAVs with nonlinear observer-based sliding mode control validated through hardware in the loop experiments. *Control Engineering Practice*, *137*, http://dx.doi.org/10.1016/j.conengprac.2023.105557.

Akers, A., Gassman, M., & Smith, R. (2006). *Hydraulic power system analysis*. CRC Press.

Al-Shuka, H. F. N., & Mikolajczyk, T. (2023). Modified virtual decomposition control for robotic mechanisms with mixed kinematic chains: A fully decentralized control algorithm. *International Journal of Dynamics and Control*, http://dx.doi.org/10.1007/s40435-023-01233-2.

Alles, P., Love, L. J., & Lanke, E. (2012). *Estimating the impact (energy, emissions and economics) of the U.S. fluid power industry*: *Technical Report December*, Oak Ridge National Laboratory.

Dalquist, S. K., & Gutowski, T. G. (2004). Life cycle analysis of conventional manufacturing techniques: Sand casting. In *Manufacturing Engineering and Materials Handling Engineering, ASME international mechanical engineering congress and exposition* (pp. 631–641). http://dx.doi.org/10.1115/IMECE2004-62599.

Dindorf, R., & Wos, P. (2020). Energy-saving hot open die forging process of heavy steel forgings on an industrial hydraulic. *Energies*, *13*, http://dx.doi.org/10.3390/en13071620.

Djordjevic, V., Tao, H., Song, X., He, S., Gao, W., & Stojanovic, V. (2023). Data-driven control of hydraulic servo actuator: An event-triggered adaptive dynamic programming approach. *Mathematical Biosciences and Engineering*, *20*, 8561–8582. http://dx.doi.org/10.3934/mbe.2023376.

Duflou, J. R., Sutherland, J. W., Dornfeld, D., Herrmann, C. H., Jeswiet, J., Kara, S., Hauschild, M., & Kellens, K. (2012). Towards energy and resource efficient manufacturing: A processes and systems approach. *CIRP Annals - Manufacturing Technology*, *61*, 587–609. http://dx.doi.org/10.1016/j.cirp.2012.05.002.

Göttlicher, G., & Pruschek, R. (1997). Comparison of CO2 removal systems for fossil-fuelled power plant processes. *Energy Conversion and Management*, *38*, S173–S178. http://dx.doi.org/10.1016/S0196-8904(96)00265-8, Proceedings of the Third International Conference on Carbon Dioxide Removal.

Guo, B., Dian, S., Zhao, T., & Wang, X. (2023). Dynamic event-driven neural network-based adaptive fault-attack-tolerant control for wheeled mobile robot system. *ISA Transactions*, *140*, 71–83. http://dx.doi.org/10.1016/j.isatra.2023.06.010.

Helian, B., Chen, Z., & Yao, B. (2021). Energy-saving and accurate motion control of a hydraulic actuator with uncertain negative loads. *Chinese Journal of Aeronautics*, *34*, 253–264. http://dx.doi.org/10.1016/j.cja.2020.12.025.

Ho, T. H., & Le, T. D. (2021). Development and evaluation of energy-saving electro-hydraulic actuator. *Actuators*, *10*, http://dx.doi.org/10.3390/act10110302.

Huang, H., Zou, X., Li, L., Li, X., & Liu, Z. (2019). Energy-saving design method for hydraulic press drive system with multi energy – saving design method for hydraulic press drive system with multi motor – pumps. *International Journal of Precision Engineering and Manufacturing-Green Technology*, *6*, 223–234. http://dx.doi.org/10.1007/s40684-019-00085-6.

Jelali, M., & Kroll, A. (2002). *Hydraulic servo-systems: Modelling, identification and control*. Springer Science & Business Media.

Koitto, T., Calonius, O., Kauranne, H., Minav, T., & Pietola, M. (2018). Enhanced energy efficiency of industrial application by direct driven hydraulic unit. In *018 global fluid power society phd symposium* (pp. 1–6). Institute of Electrical and Electronics Engineers Inc., http://dx.doi.org/10.1109/GFPS.2018.8472365.

Koivumäki, J., Zhu, W. -H., & Mattila, J. (2019). Energy-efficient and high-precision control of hydraulic robots. *Control Engineering Practice*, *85*, 176–193. http://dx.doi.org/10.1016/j.conengprac.2018.12.013.

Li, L., Huang, H., Zhao, F., Sutherland, J. W., & Liu, Z. (2017). An energy-saving method by balancing the load of operations for hydraulic press. *IEEE/ASME Transactions on Mechatronics*, *22*, 2673–2683. http://dx.doi.org/10.1109/TMECH.2017.2759228.

Lyu, L., Chen, Z., & Yao, B. (2019). Energy saving motion control of independent metering valves and pump combined hydraulic system. *IEEE/ASME Transactions on Mechatronics*, *24*, 1909–1920. http://dx.doi.org/10.1109/TMECH.2019.2930276.

Mahato, A. C., & Ghoshal, S. K. (2020). An overview of energy savings approaches on hydraulic drive systems. *International Journal of Fluid Power*, *21*, 81–118. http://dx.doi.org/10.13052/ijfp1439-9776.2114.

Meng, X., Yu, H., & Zhang, J. (2023). An EPCH control strategy for complex nonlinear systems with actuator saturation and disturbances. *Information Sciences*, *625*, 639–655. http://dx.doi.org/10.1016/j.ins.2023.01.005.

Meng, X., Yu, H., Zhang, J., & Yang, Q. (2023). Adaptive EPCH strategy for nonlinear systems with parameters uncertainty and disturbances. *Nonlinear Dynamics*, *111*, 7511–7524. http://dx.doi.org/10.1007/s11071-023-08243-x.

Niu, S., Wang, J., Zhao, J., Shen, W., & Yang, J. (2021). A novel multifunctional energy-saving electro-hydraulic servo system. In *IEEE/ASME international conference on advanced intelligent mechatronics* (pp. 314–319). IEEE, http://dx.doi.org/10.1109/AIM46487.2021.9517649.

Rana, M., Nahian, S. A., & Chowdhury, H. (2022). Energy efficiency improvement of a vertical hydraulic system. *AIP Conference Proceedings*, *2681*.

Righettini, P., Strada, R., & Cortinovis, F. (2022). General procedure for servo-axis design in multi-degree-of-freedom machinery subject to mixed loads. *Machines*, *10*.

Righettini, P., Strada, R., Valilou, S., & Khademolama, E. (2016). Nonlinear modeling and experimental validation of uni-axial servo-hydraulic shaking table. In *BATH/ASME 2016 symposium on fluid power and motion control*.

Righettini, P., Strada, R., Valilou, S., & Khademolama, E. (2017). Gray-box acceleration modeling of an electro hydraulic servo shaking table with neural network. In *IEEE/ASME international conference on advanced intelligent mechatronics* (pp. 1388–1392).

Righettini, P., Strada, R., Valilou, S., & KhademOlama, E. (2018). Nonlinear model of a servo-hydraulic shaking table with dynamic model of effective bulk modulus. *Mechanical Systems and Signal Processing*, *110*, 248–259.

Rydberg, K. -E. (2016). Hydraulic servo systems: Dynamic properties and control.

Schmidt, C., Li, W., Thiede, S., Kara, S., & Herrmann, C. (2015). A methodology for customized prediction of energy consumption in manufacturing industries. *International Journal of Precision Engineering and Manufacturing - Green Technology*, *2*, 163–172. http://dx.doi.org/10.1007/s40684-015-0021-z.

Song, X., Sun, P., Song, S., & Stojanovic, V. (2023). Finite-time adaptive neural resilient DSC for fractional-order nonlinear large-scale systems against sensor-actuator faults. *Nonlinear Dynamics*, *111*, 12181–12196. http://dx.doi.org/10.1007/s11071-023-08456-0.

Su, X., & Xiao, B. (2021). Actuator-integrated fault estimation and fault tolerant control for electric power steering system of forklift. *Applied Sciences (Switzerland)*, *11*, http://dx.doi.org/10.3390/app11167236.

Tran, D. T., Nguyen, T. N., Nguyen, X. T., & Nguyen, D. M. (2023). Synchronous PD control using a time delay estimator for a four-degree-of-freedom parallel robot in practice. *Machines*, *11*, http://dx.doi.org/10.3390/machines11080831.

Tutsoy, O., Polat, A., Colak, S., & Balikci, K. (2020). Development of a multi-dimensional parametric model with non-pharmacological policies for predicting the COVID-19 pandemic casualties. *IEEE Access*, *8*, http://dx.doi.org/10.1109/ACCESS.2020.3044929.

Wackernagel, M., & Rees, W. (1998). *Our ecological footprint: Reducing human impact on the earth, volume 9*. New society publishers.

Wang, W., Cheng, C., Zou, W., & Lu, X. (2022). Integrated energy saving and position tracking controller for the hydraulic lifting servo system. *ISA Transactions*, *119*, 196–207. http://dx.doi.org/10.1016/j.isatra.2021.02.033.

Wang, T., & Wang, Q. (2014). An energy-saving pressure-compensated hydraulic system with electrical approach. *IEEE/ASME Transactions on Mechatronics*, *19*, 570–578. http://dx.doi.org/10.1109/TMECH.2013.2250296.

Xie, X., & Li, K. (2021). Measuring total factor energy environment efficiency, saving and carbon emission reduction potential in China's food industry: Based on a meta-frontier slacks-based measure model. *Food and Energy Security*, *11*, http://dx.doi.org/10.1002/fes3.324.

Xu, Z., Liu, Y., Hua, L., Zhao, X., & Wang, X. (2020). Energy improvement of fine blanking press by valve-pump combined controlled hydraulic system with multiple accumulators. *Journal of Cleaner Production*, *257*, Article 120505. http://dx.doi.org/10.1016/j.jclepro.2020.120505.

Zare, I., Setoodeh, P., & Asemani, M. H. (2023). A controller management scheme for active fault-tolerant tracking: Linear discrete-time systems. *ISA Transactions*, *138*, 212–225. http://dx.doi.org/10.1016/j.isatra.2023.03.018.

Zhao, K., Liu, Z., Yu, S., Li, X., Huang, H., & Li, B. (2015). Analytical energy dissipation in large and medium-sized hydraulic press. *Journal of Cleaner Production*, *103*, 908–915. http://dx.doi.org/10.1016/j.jclepro.2014.03.093.

Zhou, C., Tao, H., Chen, Y., Stojanovic, V., & Paszke, W. (2022). Robust point-to-point iterative learning control for constrained systems: A minimum energy approach. *International Journal of Robust and Nonlinear Control*, *32*, 10139–10161. http://dx.doi.org/10.1002/rnc.6354.